Draft version March 3, 2024
Preprint typeset using LaTeX style emulateapj v. 12/16/11

arXiv:1709.02799v1 [astro-ph.HE] 8 Sep 2017

TYPE II SUPERNOVA SPECTRAL DIVERSITY II: SPECTROSCOPIC AND PHOTOMETRIC CORRELATIONS*.

Claudia P. Gutiérrez[1,2,3,4] Joseph P. Anderson[3], Mario Hamuy[2,1], Santiago González-Gaitan[1,5,6], Lluis Galbany[7], Luc Dessart[8], Maximilian D. Stritzinger[9], Mark M. Phillips[10], Nidia Morrell[10], Gastón Folatelli[11]

Draft version March 3, 2024

ABSTRACT

We present an analysis of observed trends and correlations between a large range of spectral and photometric parameters of more than 100 type II supernovae (SNe II), during the photospheric phase. We define a common epoch for all SNe of 50 days post-explosion where the majority of the sample is likely to be under similar physical conditions. Several correlation matrices are produced to search for interesting trends between more than 30 distinct light-curve and spectral properties that characterize the diversity of SNe II. Overall, SNe with higher expansion velocities are brighter, have more rapidly declining light-curves, shorter plateau durations, and higher ^{56}Ni masses. Using a larger sample than previous studies, we argue that 'Pd' - the plateau duration from the transition of the initial to 'plateau' decline rates to the end of the 'plateau' - is a better indicator of the hydrogen envelope mass than the traditionally used optically thick phase duration ($OPTd$: explosion epoch to end of plateau). This argument is supported by the fact that Pd also correlates with s_3, the light-curve decline rate at late times: lower Pd values correlate with larger s_3 decline rates. Large s_3 decline rates are likely related to lower envelope masses that enables gamma-ray escape. We also find a significant anticorrelation between Pd and s_2 (the plateau decline rate), confirming the long standing hypothesis that faster declining SNe II (SNe IIL) are the result of explosions with lower hydrogen envelope masses and therefore have shorter Pd values.

Keywords: supernovae: general -surveys -

1. INTRODUCTION

It is commonly accepted that Core-Collapse Supernovae (CC-SNe) are produced by the explosion of massive (> 8 M$_\odot$) stars. CC-SNe display a wide spectral and photometric variety, leading to the basis of their spectral classification. First order CC-SN classification is based on the presence or absence of hydrogen within SN spectra. SNe where hydrogen is clearly visible are called SNe II, while those without these features correspond to SNe Ib/c (Minkowski 1941; Filippenko 1997).

Initially, SNe II were classified according to the shape of the light curve: SNe with a faster decline rate are called SNe IIL, while SNe with almost constant luminosity for several months were called SNe IIP (Barbon et al. 1979). However, years later, two new classes of SNe II emerged: SNe IIn and SNe IIb. SNe IIn show narrow emission lines in their spectra, possibly due to steady interaction with a circumstellar medium (CSM; Schlegel 1990), while SNe IIb are thought to be transitional events between SNe II and SNe Ib (Filippenko et al. 1993). The overall properties of SNe IIn and SNe IIb are sufficiently distinct from 'normal' SNe II, that we do not include them for study, and they are no longer discussed in this paper.

With ever increasing numbers of SNe, new sub-classes have appeared. Blanco et al. (1987); Menzies et al. (1987); Hamuy et al. (1988); Phillips et al. (1988) and Suntzeff et al. (1988) presented analysis of SN 1987A, an object that exhibited typical characteristics of the SN II spectra, but a peculiar light curve. With this SN the 87A-like objects were introduced. Examples of these SNe can be found in Pastorello et al. (2005), Pastorello et al. (2012), and Taddia et al. (2013)[12]. Later, Pastorello et al. (2004) and more recently Spiro et al. (2014) studied the properties of low luminosity SNe II, which additionally have narrow spectral lines (indicating low expansion velocities). On the other

*This paper includes data gathered with with the 6.5 m Magellan Telescopes located at Las Campanas Observatory, Chile; and the Gemini Observatory, Cerro Pachon, Chile (Gemini Program GS-2008B-Q-56). Based on observations collected at the European Organisation for Astronomical Research in the Southern Hemisphere, Chile (ESO Programmes 076.A-0156, 078.D-0048, 080.A-0516, and 082.A-0526).

Electronic address: C.P.Gutierrez-Avendano@soton.ac.uk
[1] Millennium Institute of Astrophysics, Casilla 36-D, Santiago, Chile
[2] Departamento de Astronomía, Universidad de Chile, Casilla 36-D, Santiago, Chile
[3] European Southern Observatory, Alonso de Córdova 3107, Casilla 19, Santiago, Chile
[4] Department of Physics and Astronomy, University of Southampton, Southampton, SO17 1BJ, UK
[5] Center for Mathematical Modelling, University of Chile, Beauchef 851, Santiago, Chile
[6] CENTRA, Instituto Superior Técnico - Universidade de Lisboa, Portugal
[7] PITT PACC, Department of Physics and Astronomy, University of Pittsburgh, Pittsburgh, PA 15260, USA
[8] Unidad Mixta Internacional Franco-Chilena de Astronomía (CNRS UMI 3386), Departamento de Astronomía, Universidad de Chile, Camino El Observatorio 1515, Las Condes, Santiago, Chile
[9] Department of Physics and Astronomy, Aarhus University, Ny Munkegade 120, DK-8000 Aarhus C, Denmark
[10] Carnegie Observatories, Las Campanas Observatory, Casilla 601, La Serena, Chile
[11] Facultad de Ciencias Astronómicas y Geofísicas, Universidad Nacional de La Plata, Instituto de Astrofísica de La Plata (IALP), CONICET, Paseo del Bosque SN, B1900FWA La Plata, Argentina

[12] As the SN 87A-like objects have different light-curve properties than 'normal' SNe II, we also exclude them from our analysis.

hand, Inserra et al. (2013) analyzed a group of luminous SNe II. Lately, intermediate luminosity SNe have been also studied, supporting the wide diversity in SNe II (e.g. Roy et al. 2011; Takáts et al. 2014).

Red Super-Giant (RSG) stars with zero-age main-sequence mass ≥ 8 $M_{\odot}$ have generally been assumed as the progenitors of SNe II, with hydrodynamical modelling supporting this hypothesis (Chevalier 1976). In recent years, a significant number of direct identifications of the progenitor stars of nearby SNe IIP (e.g. Van Dyk et al. 2003; Smartt et al. 2004, 2009; Maund & Smartt 2005; Smartt 2015) suggest that RSG stars with masses of 8 - 18 $M_{\odot}$ are their progenitors, supporting initial assumptions. There is little observational constraint on the progenitor mass range of SNe IIL because only two direct identifications have been obtained (Elias-Rosa et al. 2010, 2011, but see Maund et al. 2015), however these do provide some evidence in favor of higher mass progenitors. Nevertheless, a recent analysis done by Valenti et al. (2016) with the light curves and spectra of 16 SNe II did not find any evidence for progenitor mass differences between SNe of different decline rates.

While direct detections of progenitors have constrained a relatively narrow mass range for SNe II, the same SNe show significant differences in their final explosive displays (e.g. SN 2004et, a normal SNe II, and SN 2008bk, a low luminosity event). It must therefore be that differences in stellar evolutionary processes leave the progenitors in different final states (e.g. the extent of the hydrogen envelope, the progenitor radius at explosion, the CSM) or explode with e.g. different energies, in order to produce the diversity we observe.

Theoretical studies have suggested that progenitors that explode with smaller hydrogen envelope masses produce faster declining light curves (SNe IIL), together with shorter or non-existent 'plateaus' (e.g. Litvinova & Nadezhin 1983; Bartunov & Blinnikov 1992; Popov 1993; Morozova et al. 2015; Moriya et al. 2016). An alternative study presented by Kasen & Woosley (2009) shows that a change in the explosion energy leads to a range of luminosities, velocities, and light curve durations. That is to say, higher explosion energies result in brighter events with higher expansion velocities and shorter plateaus. They also found that an increasing synthesised ^{56}Ni mass extends the length of the plateau (see also Bersten 2013). Meanwhile, Dessart et al. (2013b) using radiative-transfer models explored the properties of SNe II changing the physical parameters of the progenitor and/or the explosion (e.g. metallicity, explosion energy, radius). They found that the radius has an influence on the temperature/ionisation/color evolution (more compact objects cool and recombine faster) and in the plateau brightness, while a variation in the explosion energy leads to a variation of the plateau brightness and the plateau duration, consistent with Kasen & Woosley (2009).

To quantify the spectral and photometric diversity, a number of statistical studies of SNe II have been published. Patat et al. (1994) characterized the properties of 57 SNe II using the maximum B-band magnitude, the color at maximum and the ratio of emission to absorption (e/a) in H_{α}. They showed that faster declining events are more luminous, have shallower P-Cygni profiles and are bluer than SNe IIP. The majority of more recent studies have focused on SNe IIP. Hamuy et al. (2002) analyzed 17 SNe IIP and found that SNe with brighter plateaus have higher expansion velocities (also seen in the models of Bersten 2013. Hamuy (2003) concluded that more massive SN IIP progenitors produce more energetic explosions and in turn produce more nickel. Similar results were found by Pastorello et al. (2003) and more recently by Faran et al. (2014b). The only exception to these works about SNe IIP was published by Faran et al. (2014a), who analyzed a sample of SNe IIL. They found that faster declining SNe II (SNe IIL) are brighter than slower declining events (SNe IIP), confirming previous results.

Gutiérrez et al. (2014) and Anderson et al. (2014a) using a large sample of SNe II, analyzed the dominant line in SNe II, the H_{α} P-Cygni profile. Gutiérrez et al. (2014) using a sample of 52 SNe II (a sub-sample of that which we present here) showed that SNe with smaller values of a/e (the inverse of the ratio previously discussed by Patat et al. 1994) are brighter and have faster declining light curves. They concluded that these relationships and the diversity of a/e can be understood in terms of a varying hydrogen envelope mass at explosion epoch, together with the possibility of an influence of circumstellar interaction. Meanwhile, Anderson et al. (2014a) analyzed the blueshifted offset in the emission peaks of H_{α} of 95 SNe II. Through comparison to spectral modelling (Dessart & Hillier 2005; Dessart et al. 2013a), they argue that this behaviour is a natural consequence of the distinct density profiles found in SN ejecta.

Using a sample of 117 SNe II, Anderson et al. (2014b) (hereafter A14) studied the V-band light curve diversity of these objects. They found that SNe II with shorter plateau duration (Pd) exhibit faster decline rates (s_2 in their nomenclature). They concluded that the envelope mass at the epoch of explosion is the dominant physical parameter that explains this observed diversity. Similar results were found by Sanders et al. (2015), Valenti et al. (2016) and Galbany et al. (2016). They also found that SNe IIP and SNe IIL show a continuum in their photometric properties and it is not suitable to isolate them in two distinct classes or types.

In addition to these results, A14 found relatively high radioactive decline rates (s_3) for a significant number of SNe. In ^{56}Ni powered light curves at late times, full gamma-ray and positron trapping yields a decline rate s_3 of 0.98mag per 100 days. Higher decline rates than this value therefore suggest less efficient trapping of gamma-ray emission (or much greater explosion energies), suggesting lower mass ejecta for these SNe II.

The previous discussion shows how numerous relations between observed photometric and spectral parameters have been used to understand the SN II phenomenon. However, there are many additional parameters that have not been included in this discussion to date. Inclusion of additional parameters can aid in furthering our understanding of the underlying physics of SNe II. This motivates our current work where we study a sample of almost 1000 optical-wavelength spectra of >100 SNe II. To that aim, we have divided the analysis into two papers. In Gutierrez et al. (2017) (hereafter Paper I) we present the full description of the observations, data

reduction techniques, and the spectral properties. We also discuss the spectral matching technique to estimate the explosion epochs, the analysis of the spectral line evolution and the nature of the extra absorption component on the blue side of H_α.

Here, in this paper II we analyse the correlations between different spectral parameters defined to explore the diversity of SNe II, together with their correlation with previously defined photometric measurements. Expansion velocities, pseudo-equivalent widths (pEWs), the ratio of absorption to emission (a/e) of the H_α P-Cygni profile, and velocity decline rates are used to search for correlations with photometric parameters and between other spectral properties. We analyze spectral correlations and determine the most important properties to compare them with the photometric parameters. Our overall aim is to search for trends between different measured parameters, and then attempt to link these to the underlying physical properties of SN II progenitors.

The paper is organized as follows. Section 2 briefly describes the data employed for this analysis. In Section 3 we describe our measurement techniques. An overall current physical understanding of our different observed parameters is presented in Section 4. The full analysis is presented in Section 5. We discuss our results in Section 6 and present our conclusions in Section 7.

2. DATA

The data used in this analysis were published in A14 and Paper I. The details of the spectroscopic and photometric observations and reductions can be found in the mentioned studies. On average we have 7 spectra per SN, which are analysed together with their V-band light-curves. Details of these SNe are available in A14, Anderson et al. (2014a), Gutiérrez et al. (2014), Galbany et al. (2016) and Paper I.

A small number of SNe presented in Paper I are excluded from this work because they have insufficient spectral and/or photometric data to be useful (SNe 1988A, 1990E, 1992ad, 1992am, 1993A, 1999eg, 2002ew, 2003dq, 2004dy, 2005dw, 2005es, 2005K, 2005me, 2006bc, 2007Z, 2008F, 2009W).

3. MEASUREMENTS

The evolution of SNe II can be studied according to both spectral and photometric behaviour. At early phases the spectra exhibit the Balmer lines (H_α, H_β, H_γ, H_δ), and He I λ5876 Å. With time, the iron group lines start to appear and to dominate the region between 4000 and 6000 Å. The Ca II triplet, Na I D, and O I also emerge. The light curve at the beginning shows a fast rise to peak brightness, followed by a slight decline, which is powered by the release of shock deposited energy. Around $\sim$ 30 days post-explosion a plateau arises from the fact that the expansion of the ejecta at the photosphere compensates for the drop in optical depth. When the photospheric phase ends (around 80-120 days post explosion, A14), the transition to the nebular phase starts and the brightness drops. Once this happens, the radioactive tail phase starts. This phase is powered by the radioactive decay of ^{56}Co to ^{56}Fe. Later than $\sim$ 200 days, the spectra are dominated by forbidden lines, which are formed in the inner part of the ejecta. Much diversity is observed both in spectra and photometry, which suggests differences in the properties of the progenitor star and the explosion.

To study the diversity within SNe II we use the spectral and photometric parameters defined in Gutiérrez et al. (2014) and A14. We also define a number of additional parameters below. These measurements are chosen to enable a full characterisation of the diversity of SN II V-band light curves and optical spectra.

3.1. *Spectral measurements*

Before proceeding with our spectral analysis, below we summarise the parameters we use, as defined in Paper I:

- v: corresponds to the expansion velocity. It is measured from the minimum flux of the absorption component of P-Cygni line profile. In this analysis we measure this parameter for eleven features in the photospheric phase: H_α, H_β, Fe II λ4924, Fe II λ5018, Fe II λ5169, Sc II/Fe II λ5531, Sc II multiplet λ5663, Na I D, Ba II λ6142, Sc II λ6247, and O I λ7774. In the case of H_α, the velocity was also derived using the full-width-at-half-maximum (FWHM) of the emission component.

- $\Delta v(H_\beta)$: defined as the rate of change of the expansion velocity of the H_β feature. This parameter was measured at 5 distinct intervals (see Paper I), however here we only use the interval $50 \leq t \leq 80$ days, as this shows the highest correlation with other parameters.

- Δvel: defined as the velocity difference between H_α and Fe II λ5018, and Na I D and Fe II λ5018.

- pEW: corresponds to the absorption/emission strength of a particular line. Here, we measure the absolute value of pEW for the same features mentioned above.

- a/e: defined as the flux ratio of the absorption to emission component of H_α P-Cygni profile. This ratio is the inverse of that presented by Patat et al. (1994). We propose a/e as this deals better with weak absorption values that are shown by a number of SNe II in our sample.

While measurements were performed in all epochs at which we obtained spectra, we choose to define common epochs between SNe at 30, 50 and 80 days post explosion. An interpolation and extrapolation is used to obtain parameter values at these epochs. The values obtained by the interpolation are used when two available spectra are present $\pm$15 days around the common epoch, while the values from the extrapolation are used at $\pm$10 days. These intervals were chosen as they increase the strength of observed correlations. Using bigger intervals deteriorates the correlations because the polynomial does not produce reliable results in some cases (particularly for the pEW). At $\pm$15 and $\pm$10 days for interpolation and extrapolation, respectively, the results do not show a significant change compared to those obtained using a smaller interval. Hence, our choice of intervals is justified. To estimate the velocity at a common epoch, we

do an interpolation/extrapolation using a power law fit. For the pEW we use a low order (first or second) polynomial fit. Power law fits were found to produce satisfactory results in the case of velocity measurements, however for pEWs we found that low-order polynomials were required. For this parameter we used a low order polynomial and determined the best fit using the normalized root mean square (rms) of different orders. The errors of each measurement were obtained with the rms error fit. In summary, we are able to use spectral parameter values in 88, 84, and 59 SNe at 30, 50 and 80 days, respectively.

3.2. *Photometric measurements*

Historical separation of SNe II into distinct classes was based on photometric differences in e.g. decline rates and absolute magnitudes. Hence it is essential to include photometric parameters in our analysis for a full understanding of observed correlations and their implications for SN II physics. Here, we use the V-band photometric parameters already defined (and measured) in A14, which we now summarise:

- t_0: corresponds to the explosion epoch (see Paper I for more details of their estimation).
- t_{tran}: determined as the transition between the initial decline (s_1) and the plateau decline (s_2).
- t_{end}: corresponds to the end of the optically thick phase (i.e., the end of the plateau phase).
- t_{PT}: is the mid point of the transition from plateau to radioactive tail.
- $OPTd$: is the duration of the optically thick phase and is equal to $t_{end} - t_0$.
- Pd: is the plateau duration, defined between t_{tran} and t_{end}.
- M_{max}: defined as the initial peak in the $V-$band light-curve.
- M_{end}: defined as the absolute $V-$band magnitude measured 30 days before t_{PT}.
- M_{tail}: defined as the absolute $V-$band magnitude measured 30 days after t_{PT}.
- s_1: defined as the decline rate ($V-$band magnitudes per 100 days) of steeper slope of the light-curve.
- s_2: defined as the decline rate ($V-$band magnitudes per 100 days) of the second, shallower slope in the light curve.
- s_3: defined as the linear decline rate ($V-$band magnitudes per 100 days) of the slope in the radioactive tail part.
- ^{56}Ni mass: corresponds to the mass of radioactive nickel synthesised in the explosion. (A14 for exact details of how this was estimated).

Initial values for these parameters can be found in Table 5 in A14, however it should be noted that in this work some of these parameters have been updated: t_{tran}, $OPTd$, Pd, M_{max}, M_{end}, M_{tail}, s_1 and s_2. In the case of magnitudes it was found that stronger correlations were obtained with other parameters before any extinction corrections were made. This suggests that a) in the vast majority of cases host galaxy extinction is relatively small, and b) when we do make extinction corrections (using the absorption Na I D in A14), such corrections are not particularly accurate. Therefore, all magnitudes are being used without host galaxy extinction corrections. For t_{tran} we used the F-test to decide whether a one or two slope fit was better; A14 used the BIC criterion. The main difference resides in how the F-test penalises the number of parameters of each model (more details in Galbany et al., in prep.). This method increases the number of SNe with t_{tran} available, and in turn this increases the number of SNe for which we can define s_1 and Pd. A visual check of those SNe II showing t_{trans} using both the F-test and the BIC criterion was performed, and this gives us confidence in the use of the former in this work. All values used in the current analysis are listed in Table 1.

Besides the parameters defined by A14 we include two more parameters:

- $\Delta(B-V)$: defined as the color gradient. We measure this parameter in three different ranges: $10 \leq t \leq 20$d, $10 \leq t \leq 30$d, and $20 \leq t \leq 50$d. Color gradients are calculated by fitting a low-order polynomial to color curves and then taking the color from the fit at each epoch and calculating the gradient, $\Delta(B-V)$ by simply subtracting one epoch color from the other and dividing by the number of days of the interval.
- Cd: corresponds to the cooling phase durations (Cd), defined between t_0 and t_{tran}.

Figure 1 presents an example light curve indicating all the above defined $V-$band parameters.

4. OBSERVED PARAMETERS AND THEIR PHYSICAL IMPLICATIONS

The basic properties of the progenitor stars and explosion that have a significant influence on SN II diversity are the explosion energy (E), ejecta mass ($M_{\rm ej}$), pre-supernova radius (R_0), the ^{56}Ni mass, and progenitor metallicity (with many of these parameters likely to be directly linked to the Zero Age Main Sequence, ZAMS, mass). Theoretical works (e.g. Young 2004; Kasen & Woosley 2009; Dessart et al. 2013a) have studied how variations of these parameters influence SN II light curves and spectra. Specifically, such studies have directly linked observed parameters such as luminosities, expansion velocities and the duration of the plateau to the above physical progenitor properties.

The most commonly used parameter to link observed SN properties to progenitor characteristics has been the duration of the plateau. It has been associated to the hydrogen envelope mass of the progenitor at the moment of the explosion. Theoretical models (e.g. Litvinova & Nadezhin 1983; Popov 1993; Dessart et al. 2010a; Morozova et al. 2015; Moriya et al. 2016) have shown that

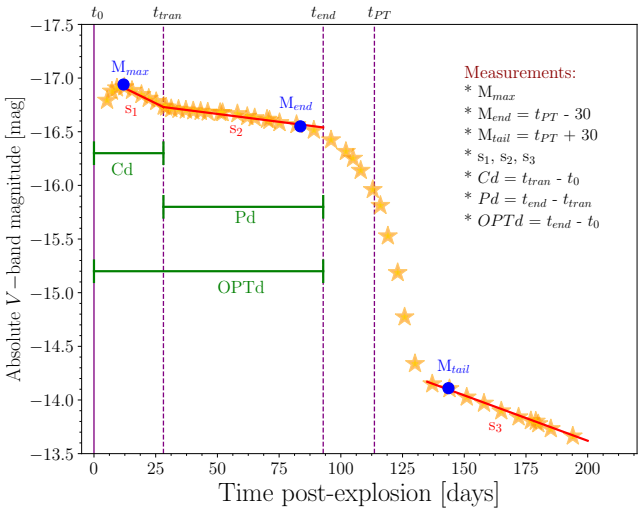


Figure 1. Example of the light-curve parameters measured for each SN within the sample in the $V-$band. Observed absolute magnitude at peak, M_{max}, M_{end} and M_{tail} are shown in blue, as applied to the dummy data points (yellow stars) of a SN II. The positions of the three measured slopes, s_1 , s_2, and s_3, are shown in red. The cooling duration (Cd), plateau duration (Pd) and optically thick phase duration ($OPTd$), are indicated in green. Four time epochs are labeled: t_0, the explosion epoch; t_{tran}, the transition from s_1 to s_2; t_{end}, the end of the optically thick phase; and t_{PT}, the mid point of the transition from plateau to radioactive tail.

the plateau duration is a good indicator of the hydrogen envelope mass in the direction that larger envelope masses produce longer duration plateaus. This can be understood as the hydrogen recombination wave taking a longer time to travel back through the ionised ejecta in SNe with a larger hydrogen envelope. Traditionally, authors have referred to the 'plateau duration' as the time from explosion to the epoch when each SN starts to transition to the nebular phase. However, such a definition then includes phases that are powered by different physical mechanisms (early-time light curves are powered by the release of shock deposited energy, while later phases during the true plateau are powered by hydrogen recombination (e.g. Grassberg et al. 1971; Chevalier 1976; Falk & Arnett 1977). In A14 two time durations were defined: $OPTd$, the optically thick phase duration, and Pd the plateau duration. The former is equivalent to the traditional definition of the plateau duration from explosion to the end of the plateau, while the latter is defined from the inflection point in the s_1 and s_2 decline rates to the end of the plateau. The newly defined Pd value should thus more accurately scale with hydrogen envelope mass, while $OPTd$ includes both effects of changing the envelope mass together with radius differences affecting the time taking for the light-curve to reach the hydrogen recombination powered s_2 decline rate. Later we provide additional evidence and arguments for this interpretation: overall correlations are stronger between Pd and other SN II measurements (particularly those other parameters linked to the envelope mass) than $OPTd$.

In addition to Pd, it was argued in A14 that decline rates during the radioactive phase, s_3, can also give an indication of the ejecta mass. The expected s_3 decline rate is 0.98 mag per 100 days assuming full trapping of the radioactive emission from ^{56}Co decay (Woosley et al. 1989).

The expansion velocity and luminosity of SNe II are both set by the explosion energy (Kasen & Woosley 2009 and Bersten 2013): more energetic explosions produce higher photospheric velocities, and in turn, brighter events. These results have been showed observationally by Hamuy & Pinto (2002); Hamuy (2003).

More recently, Dessart et al. (2010b); Dessart et al. (2013a) showed that in SNe with small progenitor radii, the recombination phase starts earlier. This would imply that the phase between the explosion and t_{tran} (cooling duration phase, Cd) is shorter in these SNe. Hence, we may expect a relation between Cd and progenitor radius. Moreover, Morozova et al. (2016) found that the early properties of the light curve are sensitive to the progenitor radius, which implies that the rise time has a relation with the radius at the time of the explosion. González-Gaitán et al. (2015) using a large sample of observed SNe II, concluded that SNe II progenitor radii are relatively small. We note however the recent results of Yaron et al. (2017), Morozova et al. (2017), Moriya et al. (2017) and Dessart et al. (2017). These investigations have provided evidence for and shown the effect of previously unaccounted for material close to the progenitor star. The interaction of the SN ejecta with such material may thus complicate the relation between early-time observations and progenitor radius.

In summary we expect that *the hydrogen envelope mass* is directly related with Pd, s_3; *the explosion energy* with the expansion velocities (vel), and the luminosities (M_{max}, M_{end}); and *the radius of the progenitor* would have some influence in Cd.

5. RESULTS

In this section we investigate the spectral and photometric diversity of SNe II through correlations. Here we present the statistics of these correlations and their respective figures. As stated above, the spectral measurements were performed in the phases where the data were available, however to characterize this diversity, the analysis is done at 30, 50 and 80 days with respect to the explosion epoch. In Table 2 we can see the average of the correlations for each parameter at 30, 50 and 80 days. The mean of these correlations shows a value of 0.323, 0.364 and 0.356 for each epoch, thus the following analysis is performed at 50 days, where more spectral measurements are available and the mean is higher. In Tables 3, and 4 the measured spectral parameters at 50 days are listed, while in Table 1 we present the photometric parameters.

5.1. *Spectral correlations in the photospheric phase*

We analyze the spectral properties of SNe II, focusing on correlations between pEWs, expansion velocities, velocity decline rate, and velocity differences. Figure 2 shows the correlation matrix of the velocity measurements at 50 days obtained by estimating the Pearson correlation coefficient. Correlation coefficients are displayed in color: darkest colors (green and purple) represent the highest correlation found with the Pearson correlation test (-1 and 1, respectively), while white colors (0) mean no correlation. These colors are presented in the lower triangle, while the upper triangle shows the Pearson correlation value (ρ). It is generally considered that correlation coefficients between 0 and 0.19 represent close to

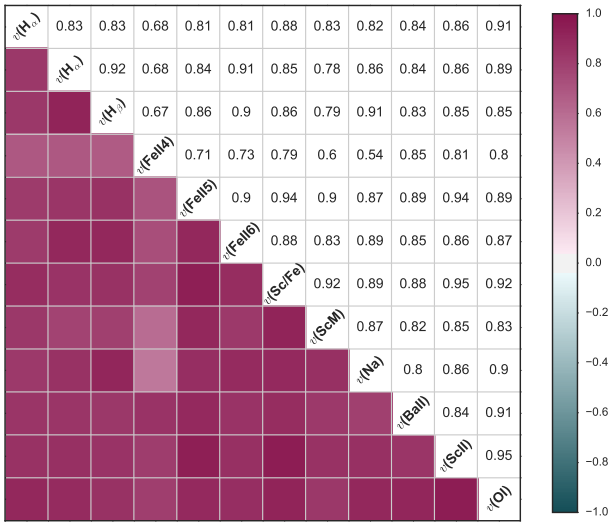


Figure 2. Correlation matrix of the individual velocity measurements at 50 days. Colors indicate the Pearson correlation coefficient ρ. The diagonal middle line shows the name of the parameter: H_α from FWHM and from the minimum absorption flux, H_β, Fe II λ4924, Fe II λ5018, Fe II λ5169, Sc II/Fe II λ5531, Sc II M λ5663, Na I D, Ba II λ6142, Sc II λ6247, and O I λ7774 velocities.

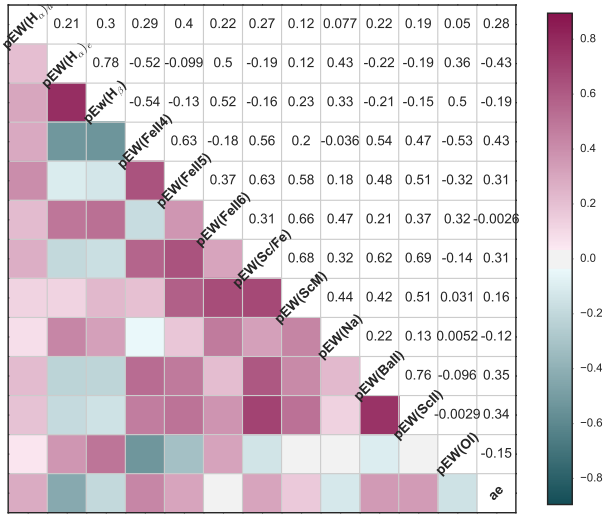


Figure 3. Correlation matrix of the individual pEW measurements at 50 days. Colors indicate the Pearson correlation coefficient ρ. The diagonal middle line shows the name of the parameter: pEW(H_α) of absorption component, pEW(H_α) of emission component, pEW(H_β), pEW(Fe II λ4924), pEW(Fe II λ5018), pEW(Fe II λ5169), pEW(Sc II/Fe II λ5531), pEW(Sc II M λ5663), pEW(Na I D), pEW(Ba II λ6142), pEW(Sc II λ6247), pEW(O I λ7774) and a/e.

zero correlation, 0.2-0.39 weak, 0.4-0.59 moderate, 0.6-0.89 strong, and 0.8-1.0 very strong (Evans 1996), while also noting the statistical significance of these correlation coefficients in many cases. We will use these descriptions for the following discussion. As shown in Figure 2, all velocities strongly correlate positively with each other, as we would expect for an homologous expansion ($v \propto r$). Taking an average, v(Sc II/Fe II) λ5531, v(O I) λ7774 and v(Sc II) λ6247 show the highest correlations with the other parameters, with values of 0.887, 0.883 and 0.875, respectively, while Fe II λ4924 shows the lowest (0.714). The Sc II λ6247 line velocities correlate strongly with Fe II λ5018 and Sc II/Fe II λ5531, with a value of $\rho = 0.94$ and $\rho = 0.95$. It is important to note that while the velocities all correlate, they are offset. In general, the differences in the velocities are related to the optical depth for each line and the proximity of the line forming region to the photosphere. As H_α displays the highest velocities, it is mostly formed in the outer shell of the ejecta and its optical depth is much larger than the Fe II lines, which are forming near to the photosphere.

Figure 3 shows the correlation matrix of the pEWs measurements at 50 days. Searching for correlations of pEWs with each other, we find that Sc II/Fe II λ5531 seems to be the dominant parameter to correlate with all the other pEWs (on average 0.404), while the pEW of H_α absorption component shows very weak correlations with other pEWs. The strongest correlations are displayed by the iron-group lines with each other. We can see moderate correlations between the pEW of O I λ7774 and H_β. In the case of a/e we find a moderate correlation only with Fe II λ4924 ($\rho = 0.43$) and anticorrelation with pEW of H_α emission ($\rho = -0.43$). While H_β shows a weak correlation with the H_α absorption component ($\rho = 0.3$), the correlation with the H_α emission component is strong, with a $\rho = 0.78$. The lack of correlation between H_α and H_β absorption features could be due to a)blending effects of Fe II, Sc II and Ba II lines with H_β, and/or b) the effects of Cachito (Paper I) on the profile of H_α.

Figures 4, 5, and 6, show the relations between the H_α, Fe II λ5169, and Na I D velocities and the pEWs for the 11 features explained above at 50 days. Checking these correlations we see that velocities correlate positively with Balmer and Na I D lines, but negatively with Fe II lines. For H_α we present the pEW of the absorption and emission component in the first two panels, respectively. In the three figures are shown five objects with the lowest velocities and smallest pEW values. Three of these SNe show signs of interaction (narrow emision lines) at early times (SN 2008bm, 2009au and 2009bu, these SNe also display abnormally low velocities for their brightness). The other two SNe are SN 2008br and SN 2002gd. In those panels plotting pEWs of Fe II λ4924, Sc II/Fe II λ5531, Sc II λ5663, Ba II λ6142, and Sc II λ6247, one can see that there are many SNe with $pEW = 0$. In these spectra we do not detect these lines.

In Figure 4 we can see that the H_α velocities do not show correlation with pEW(H_α) of the absorption component, pEW(Fe II λ5169), pEW(Sc II/Fe II λ5531), pEW(Sc II multiplet), pEW(Na I D), pEW(Ba II λ6142), and pEW(Sc II λ6247). The strongest correlations are shown with pEW(H_α) of the emission component, H_β, and anticorrelations with Fe II λ4924, and Fe II λ5018. Figures 5 and 6 show that Fe II λ5169 and Na I D velocities present more scatter in their relations than those shown by H_α velocities.

The expansion velocities with $\Delta v(H_\beta)$ show anticorrelations, which are stronger at late epochs (between 50 and 80 days) than at early phases (15 to 30 days, 15 to 50 days, and 30 to 50 days). Meanwhile, Δvel(H_α−Fe II λ5018) and Δvel(Na I D−Fe II λ5018) show correlations with the expansion velocities at 50 days (see Figure 7).

5.2. *Spectroscopic and photometric properties*

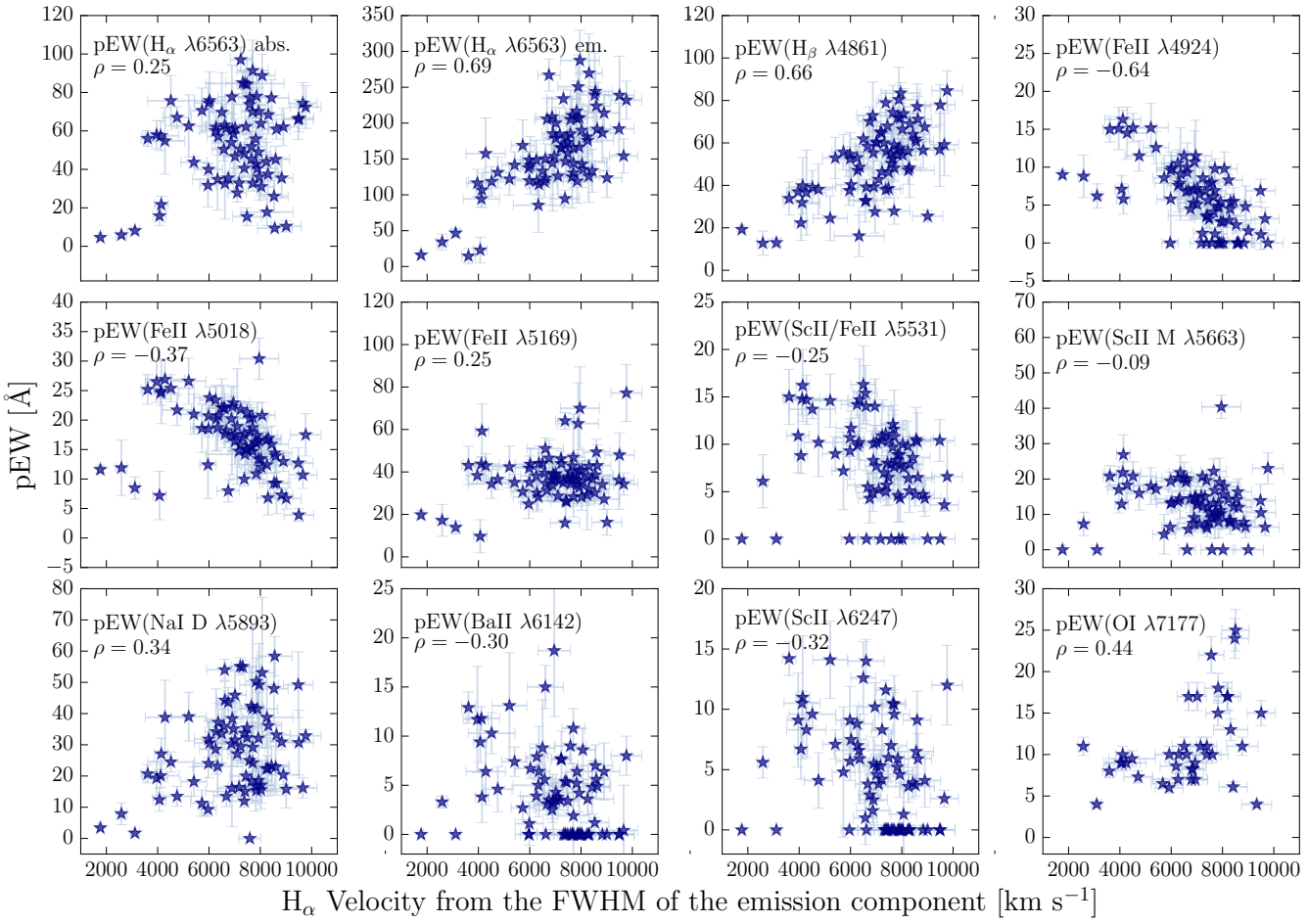


Figure 4. Relations between H$_\alpha$ velocities and the pEWs of H$_\alpha$ of absorption and emission component, H$_\beta$, Fe II λ4924, Fe II λ5018, Fe II λ5169, Sc II/Fe II λ5531, Sc II multiplet, Na I D, Ba II λ6142, Sc II λ6247, and O I λ7774. On the top left of each panel the spectral feature name is displayed, together with the Pearson correlation value.

We now present a comparison of spectroscopic and photometric properties of SNe II. While we have defined and measured 31 spectroscopic and 13 photometric parameters, here we choose a smaller number of parameters to focus on and search for correlations between them. Thus, we employ 14 spectral and 11 photometric parameters: v(H$_\alpha$) obtained from the FWHM of the emission component, v(H$_\beta$), v(Fe II 5018), v(Fe II 5169), v(Na I D), pEW(H$_{\alpha(abs)}$), pEW(H$_{\alpha(emis)}$), pEW(H$_{\beta)}$), pEW(Fe II 5018), pEW(Fe II 5169), pEW(Na I D), a/e, $\Delta v(H_\beta)$ in a range of $50 \leq t \leq 80$d, Δvel(H$_\alpha$−Fe II 5018), Δvel(Na I D−Fe II 5018), $OPTd$, Pd, Cd, M$_{max}$, M$_{end}$, M$_{tail}$, s$_1$, s$_2$, s$_3$, $\Delta(B-V)$ in a range of $10 \leq t \leq 30$ d, and the ^{56}Ni mass.

Figure 7 shows the correlation matrix of the spectroscopic parameters (obtained at 50 days from explosion) and photometric properties. Although photometric correlations have been shown in previous works (e.g. A14, Valenti et al. 2016), the incorporation of numerous spectral parameters can aid in furthering our understanding of the link between observed parameters and underlying SN II physics. As in the previous matrix of correlation, darkest colors indicate higher correlation and white colors, no correlation.

Focusing on the photometric correlations, one can see that many of these are stronger than in A14. As discussed previously, this is because some parameters have been remeasured with new techniques (Galbany et al. in prep). Interestingly, the number of SNe II with measured values of both Pd and s$_3$ show an increase from 4 in A14 to 8 in this work. As explained above, both parameters can give us an idea of the of hydrogen envelope mass at the moment of explosion, thus some relation is expected. Figure 8 shows an evident trend between both parameters, with a correlation coefficient of $\rho = -0.857$ (although we note the low number of SNe). SNe II with smaller Pd have higher s$_3$ decline rates, providing further evidence of a dominant role in defining light-curve morphology of the hydrogen envelope mass, while also providing further support for the use of Pd and s$_3$ as envelope mass indicators (given their relatively strong correlation).

From Figure 7 we also can see that Pd has a moderate correlation with velocities. Although we find a strong correlation between Pd and ^{56}Ni mass, in agreement to the theoretical predictions (e.g. Kasen & Woosley 2009), we are not in a position to support this result because the correlation is produced only with three points. However, when we include the lower limits for the ^{56}Ni mass, the correlation disappears (see top panel in Figure 9). In general, the correlations between the ^{56}Ni mass and all other parameters decrease when we use the lower limits.

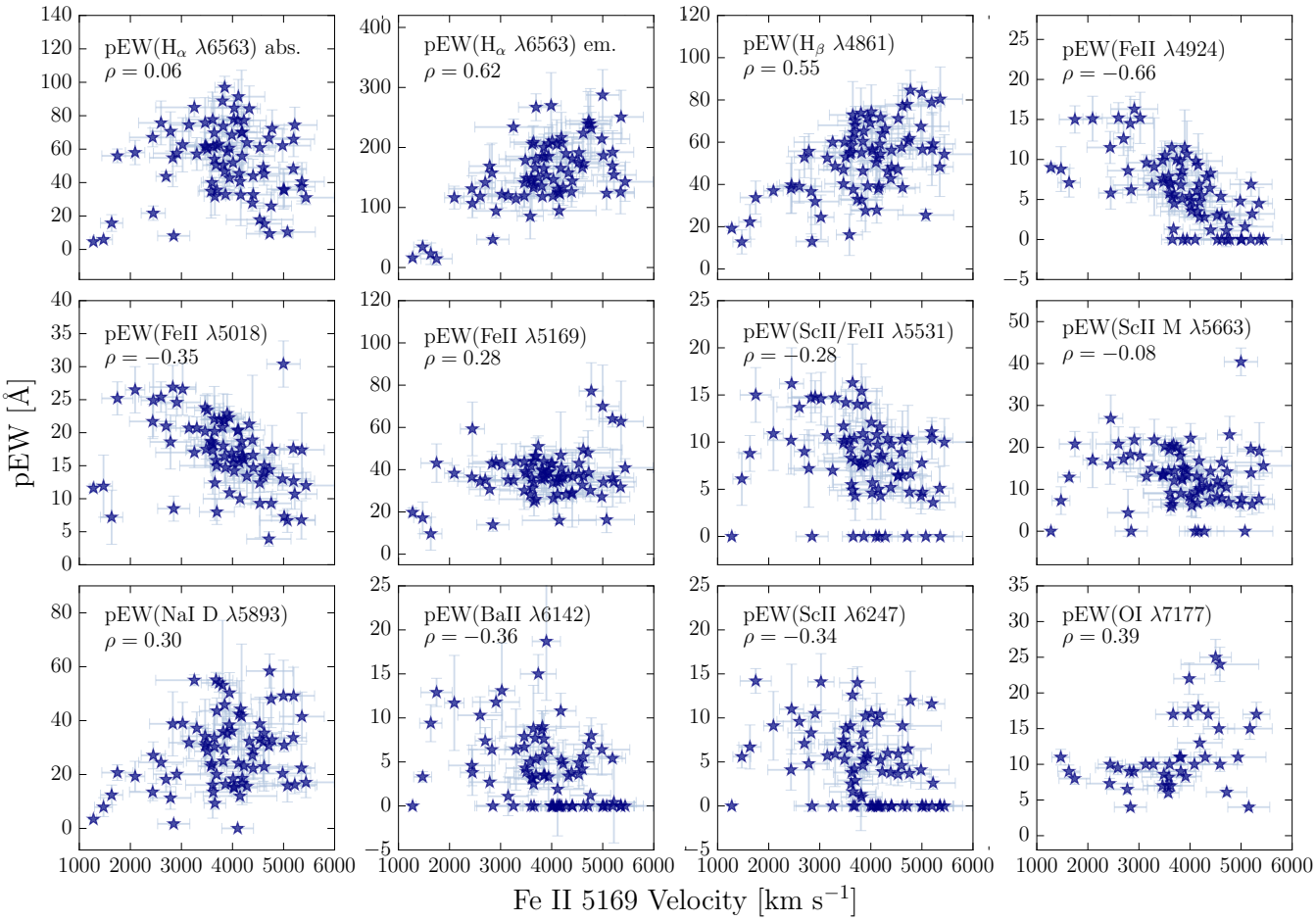


Figure 5. Same as Figure 4 but for Fe II 5169 velocities.

In the bottom panel of the same plot (Figure 9) it is possible to see how the scatter increases using the these values. The correlation goes from $\rho = -0.82$ to $\rho = -0.60$. The fact that correlations become weaker when using lower ^{56}Ni mass limits suggests that one should be careful analysing such masses when insufficient data are available for their estimation.

Continuing the analysis of Pd, we can see that it has a moderate correlation with pEW(H$_\alpha$) of the absorption component and strong correlation with a/e. The correlation coefficients are $\rho = 0.45$ and $\rho = 0.61$, respectively. In Figure 10 we present these correlations together with the best fit line obtained using the `linmix_err`[13] package (Kelly 2007) and the variance with respect to the fit line. The trend shows that SNe with shorter Pd values are brighter, have faster declining light curves, lower pEW(H$_\alpha$) of the absorption component and a/e values, and higher velocities, however the scatter is large. In many cases this scatter is significantly larger than the that which could be ascribed to the errors on individual data points. This suggests that this scatter is due to differing underlying physics driving diversity in different parameters plotted on each axis. For example, while we argue here that Pd is a good indicator of the hydrogen envelope mass, theory also predicts this parameter to be influenced by the ^{56}Ni mass (Kasen & Woosley 2009). Meanwhile, SN luminosities and velocities will be affected by both explosion energy and the ejecta/envelope mass. Interaction of the SN ejecta with CSM material at early times (e.g. Morozova et al. 2017; Moriya et al. 2017; Dessart et al. 2017) may also play a role in producing dispersion in our presented trends.

The fact that we see a significant anti-correlation between Pd and s_2 is in line with historical understanding of the nature of fast declining SNe II. If Pd is an indicator of the extent of the hydrogen envelope, then it follows that faster declining SNe II have a smaller hydrogen envelope at the epoch of explosion, consistent with previous theoretical predictions (e.g Popov 1993; Litvinova & Nadezhin 1983; Bartunov & Blinnikov 1992; Moriya et al. 2016).

In Figure 11 we test the correlation found by Hamuy & Pinto (2002) between the magnitude and the photospheric expansion velocity. Unlike Hamuy & Pinto (2002), who only used SNe IIP and the M_V in the middle of the plateau, we use all our SN II sample (no distinction between SNe IIP and SNe IIL) and the magnitude at different phases: at maximum (M$_{max}$), at the end of the plateau (M$_{end}$) and at the radioactive tail phase (M$_{tail}$). We can see that brighter events (in all phases) display higher expansion velocities, confirming the result of Hamuy & Pinto (2002). The correlations between Fe II λ5169 velocity (a proxy of the photospheric ve-

[13] A Bayesian approach to linear regression with errors in both X and Y.

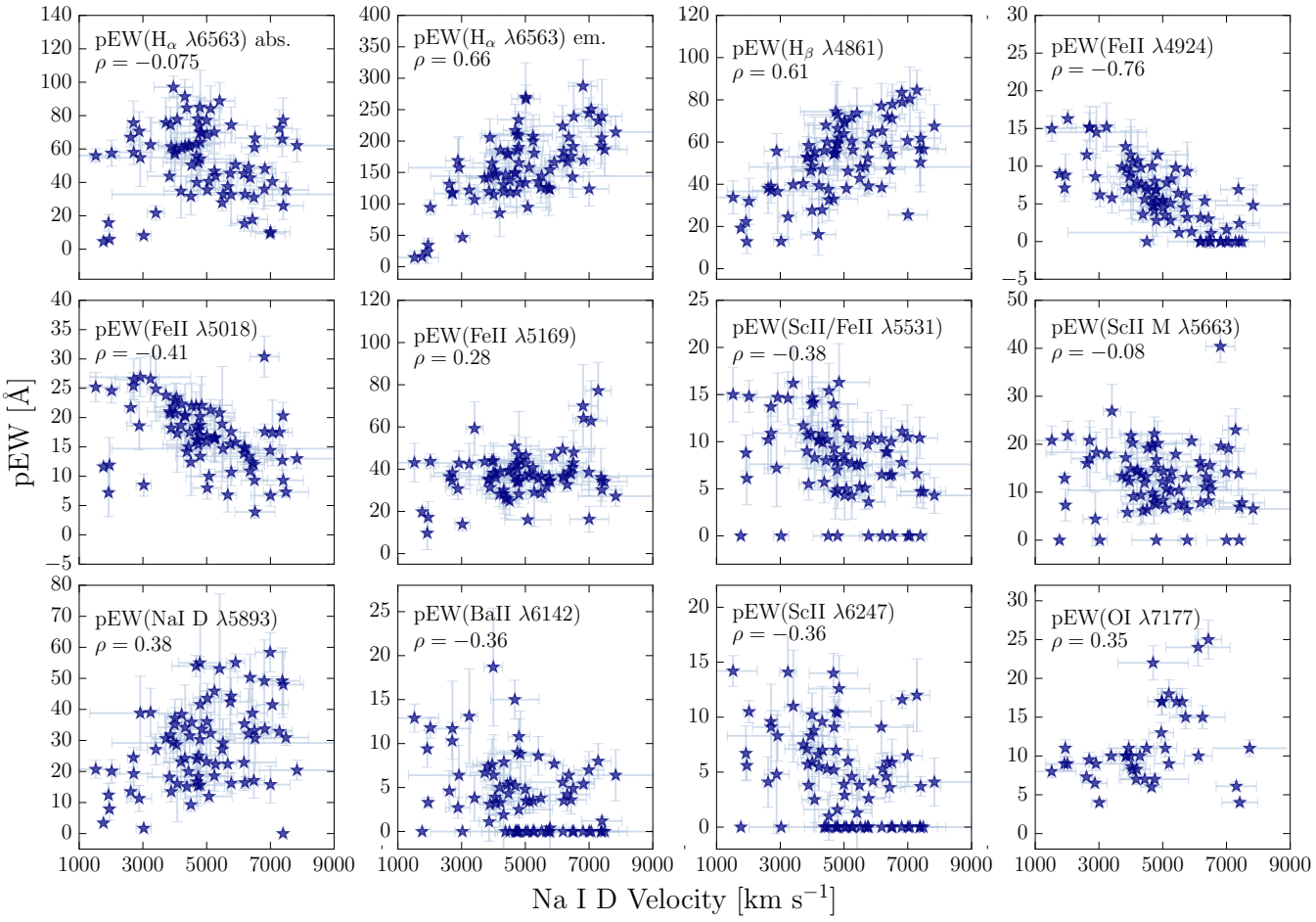


Figure 6. Same as Figure 4 but for Na I D velocities.

locity) at 50 days and luminosity during the optically thick phase are moderate ($\rho = -0.54$ with M_{max} and $\rho = -0.45$ with M_{end}), and strong ($\rho = -0.62$) in the radioactive tail phase. However, we again note the outliers in these figures, where the correlation appears much stronger when removing these events (the outliers are mainly the same SNe discussed previously that show abnormal spectral properties). Interestingly, correlations are higher between spectral velocities and M_{max} than with M_{end} (the Standardized Candle Method, SCM, is generally applied using a magnitude during the plateau, more similar to M_{end}). Analysing the variance along the best fit line, we find that the dispersion in velocity is larger in brighter SNe. Although the magnitudes and the expansion velocities are both directly related with the explosion energy, this scatter could suggest an extra influence by an external parameter. In the three main outliers in this plot we observe signs of weak interaction at early times (see spectra presented in Paper I). In these three obvious cases, but also in other more 'normal' SNe II, interaction could play a role in influencing both the magnitudes and velocities observed. CSM interaction is likely to produce more dispersion within brighter SNe II as it will generally increase the early-time luminosity while possible decreasing velocities, hence pushing SNe II away from the classic magnitude-velocity relation. In addition, the unaccounted for effects of host galaxy reddenning will produce additional dispersion.

The expansion velocities show a strong correlation with ^{56}Ni mass (see Figure 12). This suggests that more energetic explosions produce more ^{56}Ni. Additionally, the luminosities have a very strong correlation with the ^{56}Ni mass, which supports the results obtained by Hamuy (2003); Pejcha & Prieto (2015a,b) and more recently by Müller et al. (2017). It is possible to see that these three parameters (luminosities, velocities and ^{56}Ni mass) are related and they can be explained through a correlation of both parameters with explosion energy: more energetic explosions produce brighter SNe with faster velocities (as shown in the models of Dessart et al. 2010a). For those correlations that we do not plot, the reader can see the strength of correlation in Figure 7.

Figure 13 presents correlations between M_{max} and the pEWs of H_α, Fe II 5018, and Na I D. We observe a weak correlation with the pEW(H_α) absorption component, a moderate ($\rho = 0.54$) correlation with pEW(Fe II 5018), and no correlations with pEW(Na I D).

In Figure 14 we repeat the correlations presented by A14, which show that a faster declining SN at one epoch is generally also a fast decliner at other epochs. Although the correlation of s_3 and M_{max} is moderate, it is driven by an outlier event, SN 2006Y. As A14 noted, this SN presents an atypical behaviour in photometry, but here we confirm its strange behaviour in the spectra. If we remove this SN from the analysis, the correlations decrease significantly. The correlations between s_3 and the

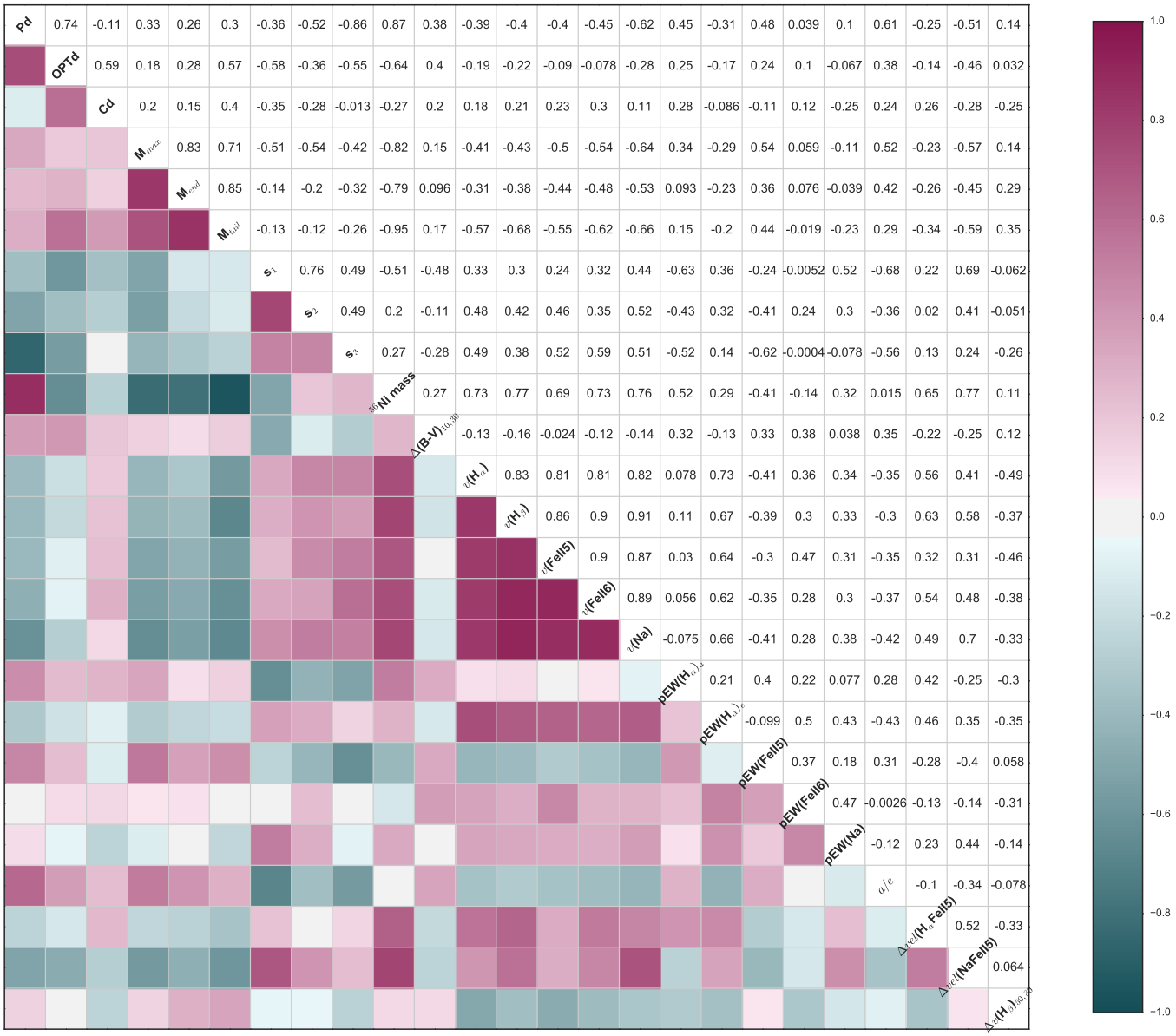


Figure 7. Correlation matrix of the individual spectral and photometric parameters at 50 days. Colors indicate the Pearson correlation coefficient ρ. In the diagonal line is shown Pd: plateau duration; $OPTd$: optically thick duration; Cd: cooling duration; M_{max}: magnitude at maximum; M_{end}: magnitude at the end of the plateau; M_{tail}: magnitude in the radioactive tail phase; s_1: initial decline; s_2: plateau decline; s_3: radioactive tail decline; ^{56}Ni mass: nickel mass; $\Delta(B-V)_{10,30}$: color gradiente between 10 and 30 days from explosion; $v(H_\alpha)$: H_α velocity obtained from the FWHM of the emission component; $v(H_\beta)$: H_β velocity; v(FeII5): Fe II 5018 velocity; v(FeII6): Fe II 5169 velocity; v(Na): Na I D velocity, $pEW(H_\alpha)_a$: pEW of H_α absorption component; $pEW(H_\alpha)_e$: pEW of the H_α emission component, $pEW(H_\beta)$: pEW of H_β, pEW(FeII5): pEW of Fe II 5018, pEW(FeII6): pEW of Fe II 5169; pEW(Na): pEW ofNa I D, a/e: ratio of absortion to emission component of H_α P-Cygni profile; $\Delta vel(H_\alpha$FeII5): $\Delta vel(H_\alpha-$Fe II 5018), Δvel(NaFeII5): Δvel(Na I D$-$Fe II 5018); and $\Delta v(H_\beta)_{50,80}$: $\Delta v(H_\beta)$ in a range of $[+50, +80]$ days.

velocities are moderate. In the last panel of Figure 14 the correlation between s_3 and the pEW(Fe II 5018) is presented, which, like M_{max} is driven by SN 2006Y. Summarizing, s_3 has weak correlations with the pEWs and the magnitudes.

6. DISCUSSION

Using numerous defined spectral and photometric parameters we have searched for correlations between different observed properties of SNe II. We argue that Pd is a better parameter than $OPTd$ for constraining the pre-SN hydrogen envelope mass. Our analysis shows a strong correlation between Pd and s_3, arguing that both of these parameters are strongly linked to the hydrogen envelope mass/ejecta mass. While expansion velocities and SN II magnitudes display a significant degree of correlation, they show only weak/moderate correlations with Pd and s_3, suggesting that explosion energy - observed through diversity in velocities and luminosity - and hydrogen envelope mass vary somewhat independently between SNe II.

We now qualitatively compare our results with those found in previous studies, both observational and theoretical, attempting to tie these correlations to the

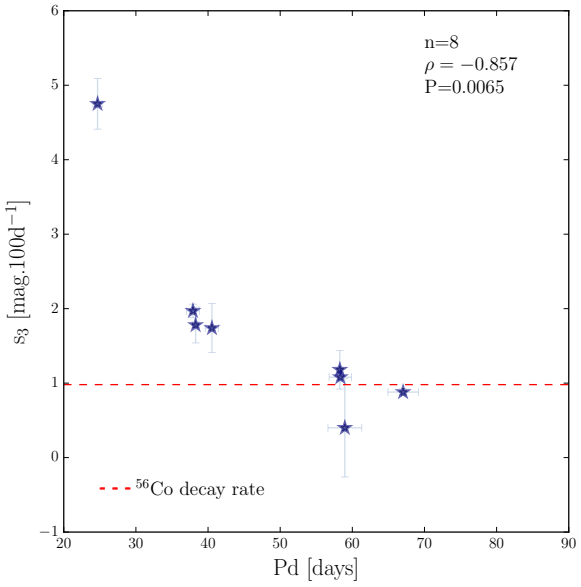


Figure 8. Correlation between *Pd* vs. s_3. On the top of the figure: n = number of events, ρ = Pearsons correlation coefficient, and P = probability of detecting a correlation by chance. The dashed horizontal line shows the expected decline rate on the radioactive tail, assuming full trapping of gamma-rays from ^{56}Co to ^{56}Fe decay.

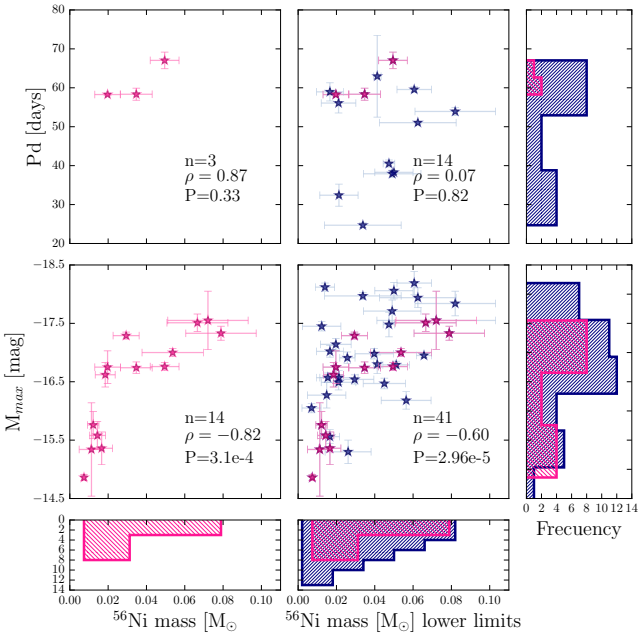


Figure 9. *Top:* Correlations between *Pd* and the ^{56}Ni mass with the accurate values (left) and including the lower limits (right). *Bottom:* Correlations between M_{max} and the ^{56}Ni mass with the accurate values (left) and including the lower limits (right). The accurate values for ^{56}Ni mass are display in red. On the top of each figure: n = number of events, ρ = Pearsons correlation coefficient, and P = probability of detecting a correlation by chance. Histograms along the x and y-axes show the distributions of the various parameters plotted on each axis. Each histogram displays the ρ_{val} found using the Shapiro-Wilk normalization. When the $\rho_{val} > 0.05$, the dataset comes from a population which has a normal distribution.

underlying physics of SNe II.

6.1. *The influence of explosion energy*

Hamuy & Pinto (2002) found that the luminosity of the SNe IIP correlates with the photospheric velocity (Fe II velocity) at 50 days from explosion. Brighter SNe II have higher ejecta expansion velocities. This correlation has enabled the use of SNe II as distance indicators. In Figure 11 we show the same relation, but in generalized form; velocities correlate with SN II brightness at all epochs. In addition, we show that this luminosity-velocity correlation is stronger at peak brightness (M_{max}) than during the plateau. Dessart et al. (2013a) has shown that more energetic explosions produce more ^{56}Ni mass, brighter SNe II with faster expanding velocities. This is consistent with our results, and suggests that explosion energy is indeed a primary parameter that influences SN II diversity, and that is traced through SN II brightness, velocities and ^{56}Ni mass.

6.2. *The influence of hydrogen envelope mass*

According to theoretical models faster declining SNe II can be explained by the explosion of stars with low hydrogen envelope mass (e.g. Litvinova & Nadezhin 1983; Bartunov & Blinnikov 1992; Popov 1993 and Moriya et al. 2016). As discussed previously, differences in envelope mass are likely to directly affect the length of the plateau, *Pd* (we again stress the difference between this parameter and *OPTd*, with the latter traditionally being assumed to be related to the envelope mass). This is because the plateau, *Pd*, is powered by the recombination of hydrogen in the expanding ejecta, and the lower the hydrogen envelope mass the quicker the recombination wave reaches its inner edge. The fact that *Pd* also correlates with s_3 (Figure 8) further supports this view, given that higher s_3 can be interpreted as being due to a lower ejecta mass (A14) that can trap the radioactive emission (which is powering the light-curve at these late epochs). With respect to faster declining SNe II, we observe a significant trend in that SNe II with higher s_2 have smaller *Pd* values, implying that the former is indeed related to the hydrogen envelope mass as has been predicted and discussed for many years. Recent observational works (e.g. A14, Valenti et al. 2016) suggested that the phase between the explosion date and the end of the plateau (historically known as the plateau duration, but here named *OPTd*) is the key parameter constraining the envelope mass. However, *Pd* shows higher degrees of correlation with other parameters, in particular s_2 and s_3. This suggests that *Pd* is indeed a better tracer of envelope mass than *OPTd*. In addition, we find that a/e shows strong and moderate correlation with *Pd* and s_3 respectively, suggesting that this spectral parameter is also a useful tracer of envelope mass (as already argued in Gutiérrez et al. 2014).

From the the correlation matrix (Figure 7) we can observe stronger relations between *Pd* and s_2, as well as with the expansion velocity, than between *OPTd* and the same parameters. This is because all these parameters are measured during the recombination phase, where they have similar physical conditions. On the other hand, *OPTd* conveys information on the physical parameters

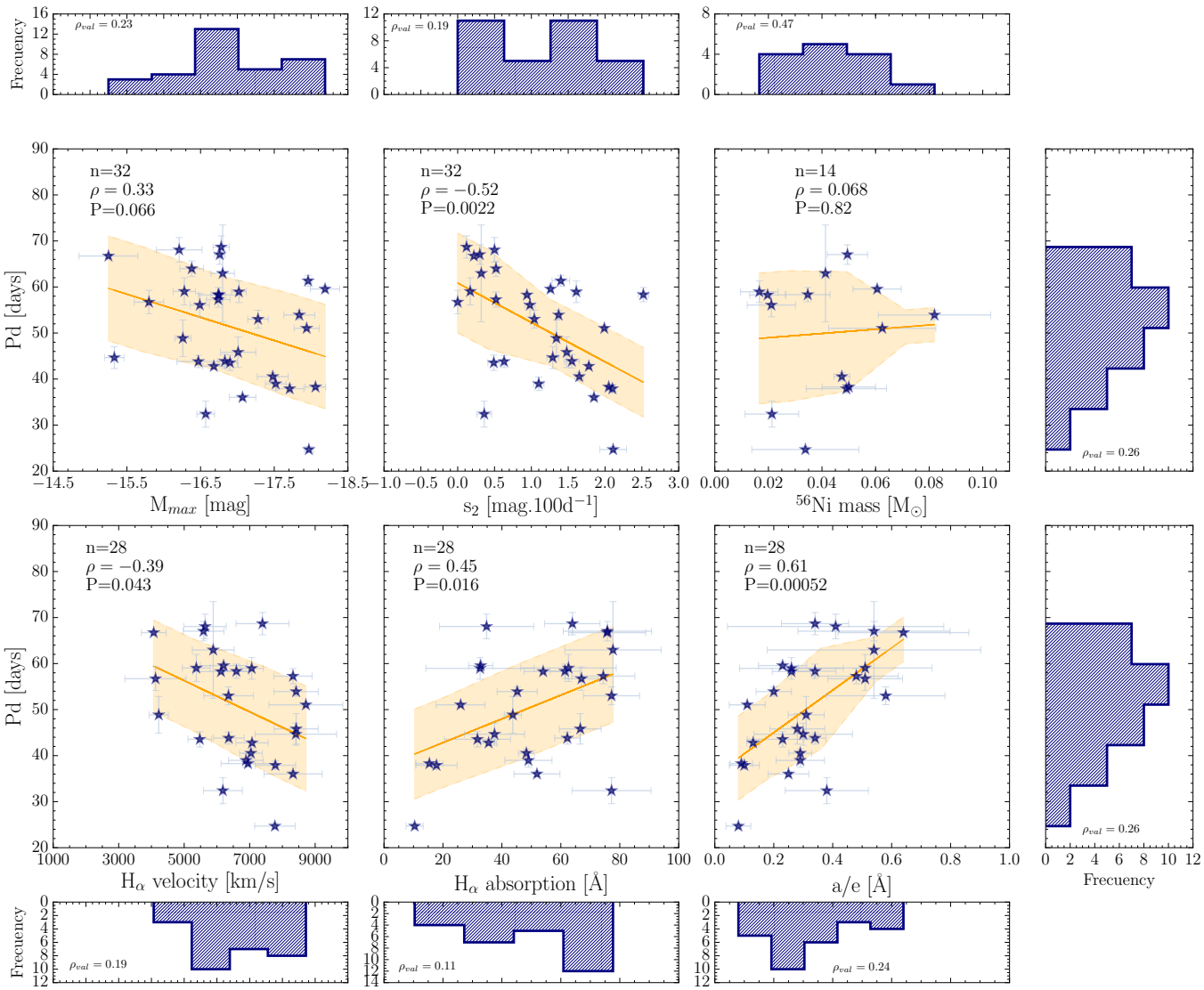


Figure 10. Correlations between Pd and six different parameters: M_{max}, s_2, ^{56}Ni mass, H_α velocity, pEW of H_α absorption component, a/e. On the top of the figure: n = number of events, ρ = Pearsons correlation coefficient, and P = probability of detecting a correlation by chance. In addition, each plot shows the corresponding best fit (`linmix_err`; Kelly 2007) as solid orange line, while the orange shaded area indicates the variance with respect to the fit line. Histograms along the x and y-axes show the distributions of the various parameters plotted on each axis. Each histogram displays the ρ_{val} found using the Shapiro-Wilk normalization. When the $\rho_{val} > 0.05$, the dataset comes from a population which has a normal distribution.

that dominate the early phases of the light curve, plus the hydrogen envelope recombination. Consequently the correlations are weaker.

In Figure 7 we can see that ^{56}Ni mass shows a strong correlation with Pd, while with $OPTd$ display an anticorrelation. Analysing these findings (Figure 15), we can see that the relation between ^{56}Ni mass and the Pd is produced by only three measurements, and therefore the probability of this correlation being real is very small (P=0.33). In the case of the $OPTd$–^{56}Ni mass plot, this anti-correlation is driven by a number of outliers.

From Figure 7, we also see that $OPTd$ has stronger correlations with Cd, s_1 and M_{tail} than with Pd. The strong relation between $OPTd$ and Cd is expected because the former, by definition, includes the latter one (the same applies to $OPTd$ and Pd; see the $OPTd$ definition in Figure 1). However, Pd and Cd are not related, because they are most likely associated with different physical properties of SNe II. Between $OPTd$ and s_1 the correlation is moderate, but again, it is driven by the physical parameters that dominate the early phases of the light curve, which, by definition, are included in $OPTd$. One interesting correlation is displayed between $OPTd$ and M_{tail}: SNe II with larger $OPTd$ values are fainter in the radioactive tail phase. This relation may be understood given that the epoch of the M_{tail} measurement directly arises from the length of $OPTd$. This means that, if the optically thick phase takes more time, the M_{tail} will be measured later, which in turn, implies fainter magnitudes (for the same ^{56}Ni mass that is powering the late-time LC). This suggests that, the correlation between $OPTd$ and M_{tail} is essentially based on the total duration of the optically thick phase, i.e., the photospheric phase.

In summary, we observe three key SN II parameters that we believe are strongly related to the extent of the hydrogen envelope mass at the moment of explosion: Pd,

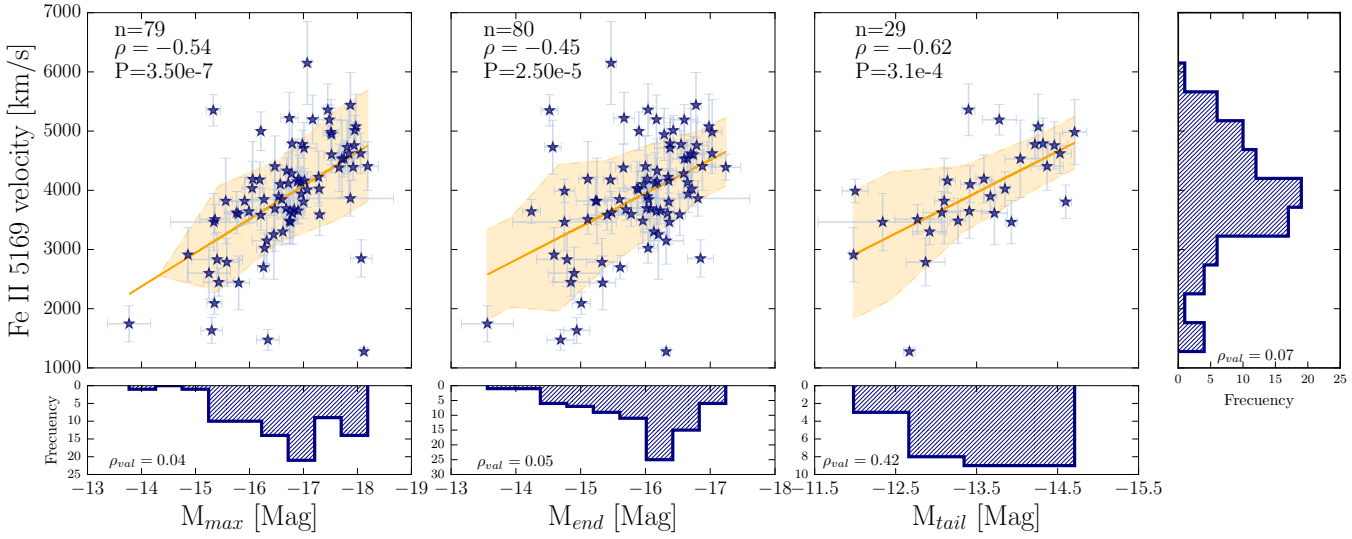


Figure 11. Correlations between (Fe II λ5169) velocity and the magnitudes: M_{max}, M_{end} and M_{tail}. In the top left of each plot the following values are given: n = number of events, ρ = Pearsons correlation coefficient, and P = probability of detecting a correlation by chance. In addition, each plot shows the corresponding best fit (`linmix_err`; Kelly 2007) as solid orange line, while the orange shaded area indicates the variance with respect to the fit line. Histograms along the x and y-axes show the distributions of the various parameters plotted on each axis. Each histogram displays the ρ_{val} found using the Shapiro-Wilk normalization. When the $\rho_{val} > 0.05$, the dataset comes from a population which has a normal distribution.

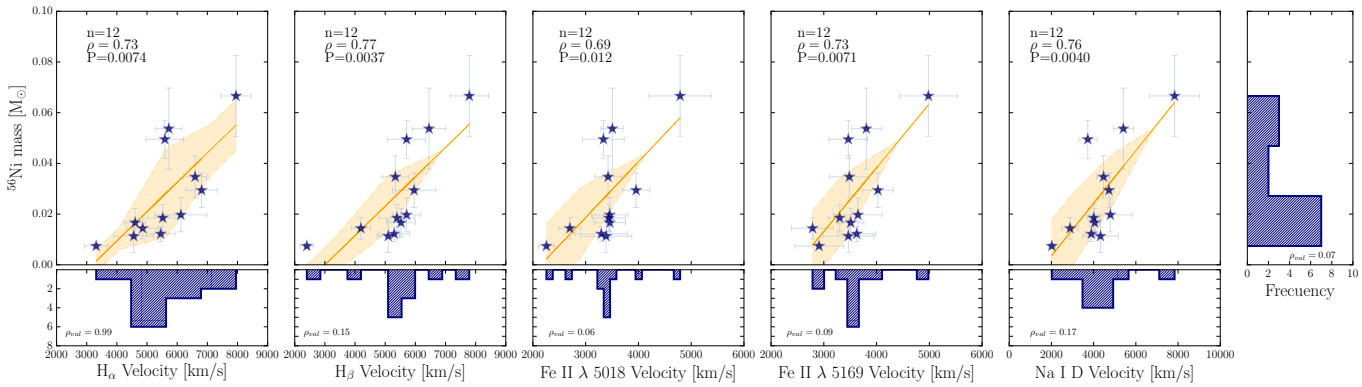


Figure 12. Correlations between ^{56}Ni and the expansion velocities. On the top of the figure: n = number of events, ρ = Pearsons correlation coefficient, and P = probability of detecting a correlation by chance. In addition, each plot shows the corresponding best fit (`linmix_err`; Kelly 2007) as solid orange line, while the orange shaded area indicates the variance with respect to the fit line. Histograms along the x and y-axes show the distributions of the various parameters plotted on each axis. Each histogram displays the ρ_{val} found using the Shapiro-Wilk normalization. When the $\rho_{val} > 0.05$, the dataset comes from a population which has a normal distribution.

s_3, and a/e.

6.3. *The influence of explosion energy on the strength of spectral lines*

Figures 4, 5 and 6 display some interesting trends. While the strength of each correlation is complicated by the obvious outliers together with those SNe where no spectral line detection was made, in general it seems that expansion velocities correlate positively with the strength of the Balmer lines and Na I D, and negatively with the strength of metal lines. The strength of metal lines at any given epoch is most strongly related to the temperature of the line forming region. We therefore conclude that more energetic explosions produce SNe II that stay at higher temperatures for longer leading to lower metal-line pEWs. With respect to the Balmer lines (at least the emission component of H_α and the absorption component of H_β) this would then imply that more energetic explosions lead to relatively stronger line strengths. The exact physical interpretation of this is unclear. Brighter, i.e., more energetic SNe II also display weaker metal lines (Figure 7 and specifically Figure 13 bottom middle panel). Finally, we also note that differences in progenitor metallicity will also affect the strength of metal lines within spectra, as argued by Dessart et al. (2014) and Anderson et al. (2016) (but probably to a lower degree, at least in the current sample).

6.4. *H_α P-Cygni diversity*

A large diversity in the H_α P-Cygni profile had been shown by Patat et al. (1994) and Gutiérrez et al. (2014). They found that SNe II with smaller a/e values are brighter, and have higher velocities and steeper decline rates. With our analysis at 50 days, we confirm these results, however the correlations presented here are of lower strength than those in Gutiérrez et al. (2014). This is most likely due to the epoch of the measurements,

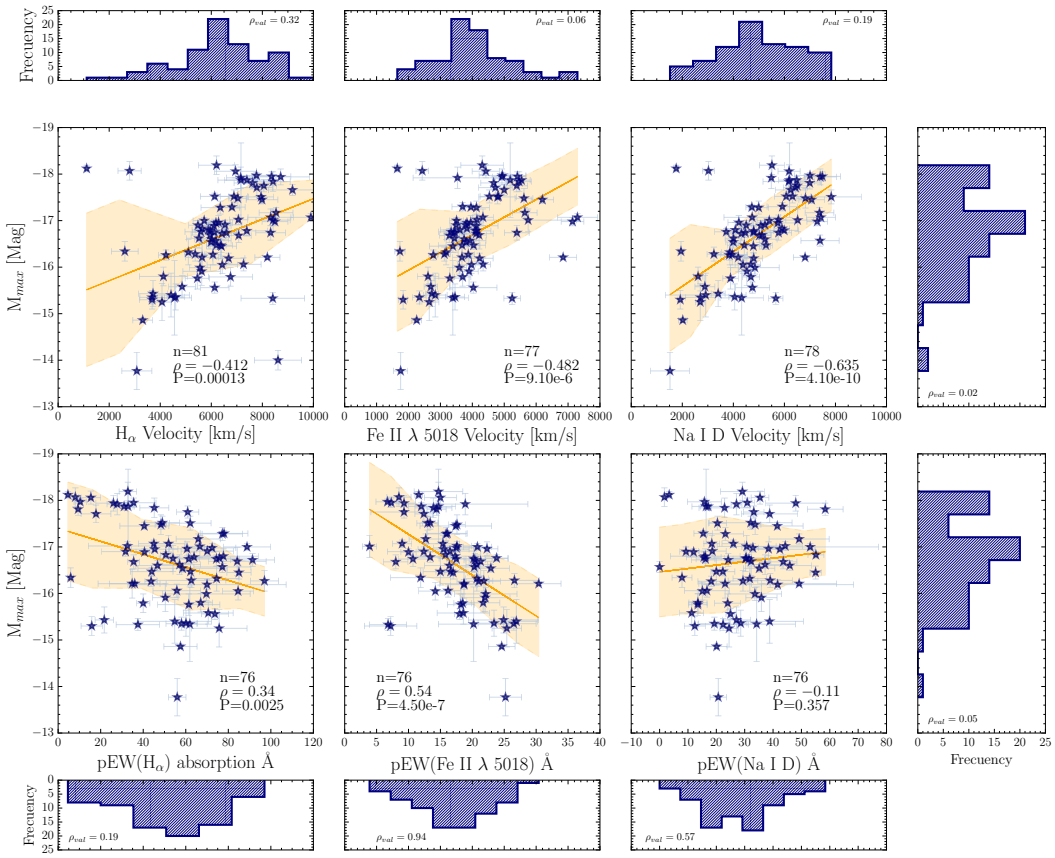


Figure 13. Top panel: Correlations between M_{max} and the expansion velocities. **Bottom panel:** Correlations between M_{max} and the pEWs. On the top of the figure: n = number of events, ρ = Pearsons correlation coefficient, and P = probability of detecting a correlation by chance. In addition, each plot shows the corresponding best fit (`linmix_err`; Kelly 2007) as solid orange line, while the orange shaded area indicates the variance with respect to the fit line. Histograms along the x and y-axes show the distributions of the various parameters plotted on each axis. Each histogram displays the ρ_{val} found using the Shapiro-Wilk normalization. When the $\rho_{val} > 0.05$, the dataset comes from a population which has a normal distribution.

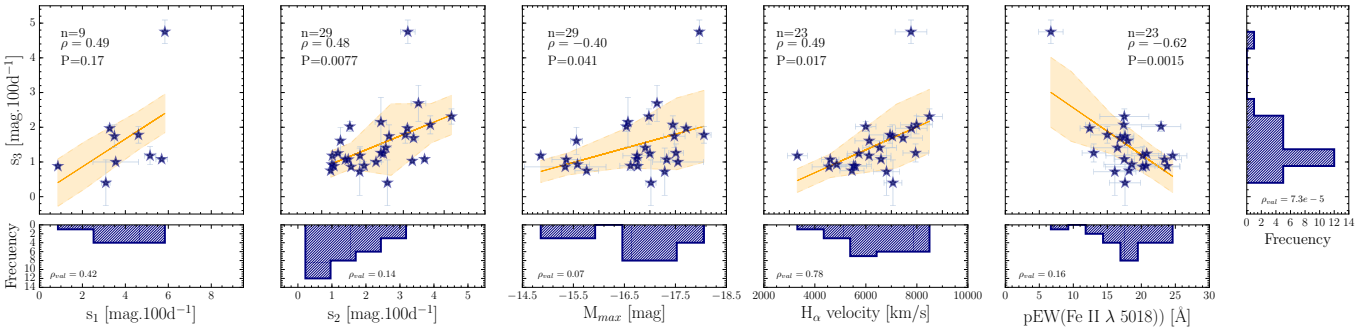


Figure 14. Correlations between s_3 and five different parameters: s_1, s_2, M_{max}, H_α velocity, pEW(Fe II λ 5018). On the top of the figure: n = number of events, ρ = Pearsons correlation coefficient, and P = probability of detecting a correlation by chance. Histograms along the x and y-axes show the distributions of the various parameters plotted on each axis. Each histogram displays the ρ_{val} found using the Shapiro-Wilk normalization. When the $\rho_{val} > 0.05$, the dataset comes from a population which has a normal distribution.

where in Gutiérrez et al. (2014) measurements were made at $t_{tran+10}$ (where t_{tran} is the transitional epoch between s_1 and s_2). Here we chose to use epochs with respect to explosion to measure our spectral parameters. This enables us to analyse the full range of events within our sample (in many SNe II it is not possible to define t_{tran}). The difference in correlation strength therefore arises from the measurements in Gutiérrez et al. (2014) being made when SNe II are likely to be under more consistent physical conditions. Here, using an epoch of 50 days post explosion different SNe are at different phases of their evolution.

It has previously been argued that the H_α P-Cygni diversity is directly related to the hydrogen envelope mass (Schlegel 1996; Gutiérrez et al. 2014). The results we present here also support this view, with the absorption component of H_α - and in particular the absorption in relation to the emission, a/e - showing correlation with both Pd and s_3, parameters that we have already argued are direct tracers of the envelope mass. We also

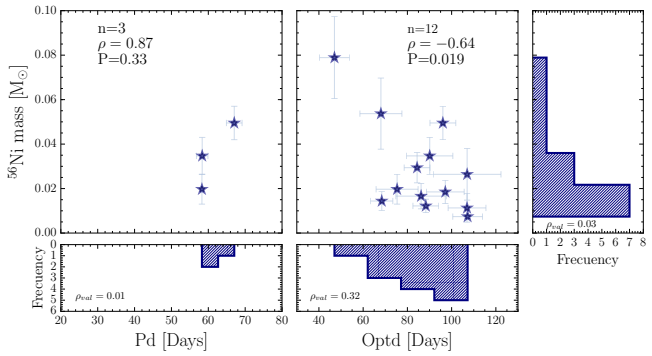


Figure 15. Correlations between ^{56}Ni mass and Pd (on left) and $OPTd$ (on right). On the top of the figure: n = number of events, ρ = Pearsons correlation coefficient, and P = probability of detecting a correlation by chance. Histograms along the x-and y-axes show the distributions of the various parameters plotted on each axis. Each histogram displays the ρ_{val} found using the Shapiro-Wilk normalization. When the $\rho_{val} > 0.05$, the dataset comes from a population which has a normal distribution.

note however that the measurement of H_α absorption is complicated by the detection and diversity of Cachito (Paper I). It is quite possible therefore that vast majority of the underlying diversity of H_α morphology is determined by the hydrogen envelope mass, but complications in the latter's measurement introduce much of the dispersion we see (in e.g. Figure 10, bottom right).

6.5. *Other comparisons*

As discussed in Patat et al. (1994), A14 and more recently Valenti et al. (2016) and Galbany et al. (2016), we find that faster declining SNe II are brighter events (see Figure 10). In addition, we also find that SNe II with brighter luminosities have greater expansion velocities and produce more ^{56}Ni. In Figure 12 and 13 we show a few examples of these correlations. Similar results were found by several authors in observational (e.g. Hamuy 2003; Spiro et al. 2014; Valenti et al. 2016; Müller et al. 2017) and theoretical (e.g. Kasen & Woosley 2009) works.

Theoretical models show and increase in the ^{56}Ni mass leads to an increase in the plateau duration (e.g.Kasen & Woosley 2009 and Nakar et al. 2016). We do not find any observational evidence for such a trend. There are only 3 data points in the correlation between Pd and ^{56}Ni, therefore strong conclusions are not warranted. If we include lower-mass ^{56}Ni limits we also see no evidence for correlation. This may suggest that observationally Pd does not depend on the mass of ^{56}Ni mass. However, given the inclusion of lower-mass ^{56}Ni limits, this warrants caution.

Many authors have found (e.g. Dessart & Hillier 2011) that SN II color evolution could be related with the radius of the progenitor star. Although we include the color gradient ($\Delta(B-V)$) between 10–30 days post-explosion in our analysis, we do not find significant correlations associated to this parameter. However, we do note low-level correlation between $\Delta(B-V)$ and the strength of Fe II λ5018 and Fe II λ5169 (Figure 7), in the direction one would expect: SNe II that cool more quickly (higher $\Delta(B-V)$) display stronger metal-line pEWs. Cd also does not display significant correlation with other parameters. While above we linked Cd to progenitor radius, as predicted by Dessart et al. (e.g. 2013a), the direct influence of radius on Cd is complicated by any presence of CSM close to the progenitor and may explain the lack of correlations.

Dessart et al. (2014) showed that differences in metallicity strongly influence in the SN II spectra, more precisely in the strength of the metal lines. Anderson et al. (2016) supported this result showing a correlation between the strength of Fe II λ5018 with the oxygen abundance of host H II regions. They showed that SNe II exploding in lower metallicity regions have lower iron absorption. Looking for relations with the pEW(Fe II λ5018), we find a correlation of 0.48 with the Pd and -0.62 with s_3. Assuming that the pEW(Fe II λ5018) gives an idea of the metallicity where the SN explode, this correlation would mean that higher metallicity produce SNe with a longer plateau, which is in the opposite direction of the predictions (e.g. Dessart et al. 2013a). However, when we correlate Pd with the oxygen abundance determined by Anderson et al. (2016), we do not find any relation. As in Anderson et al. (2016) we therefore conclude that (at least in the current sample), the strength of metal lines is dependent more on temperature than progenitor metallicity.

7. CONCLUSIONS

In this work we have presented an analysis of correlations between a range of spectral and photometric parameters of 123 SNe II, with the purpose of understanding their diversity. To study this diversity, we use the expansion velocities and pseudo-equivalent widths for eleven features in the photospheric phase (from explosion to $\sim$ 120 days): H_α, H_β, Fe II 4924, Fe II λ5018, Fe II λ5169, Sc II/Fe II λ5531, Sc II M, Na I D, Ba II λ6142, Sc II λ6247, and O I λ7774; the ratio absorption to emission (a/e) of the H_α P-Cygni profile; the velocity decline rate of H_β ($\Delta v(H_\beta)$) and the velocity difference between H_α and Fe II λ5018, and Na I D and Fe II λ5018 (Δvel). From the light curves we employed three magnitude measurements at different epochs (M_{max}, M_{end}, M_{tail}); three decline rates (s_1, s_2, s_3); three time durations ($OPTd$, Pd, Cd); the ^{56}Ni mass, and the color gradient, $\Delta(B-V)$. We searched for correlations at 30, 50 and 80 days, finding that correlations are stronger at 50 days post-explosion. We suggest this happens because at 50 days SNe II are under similar physical conditions: at 30 and 80 days not all SNe II are in the same stage, some are in the cooling (at early phases) and some are in the transition to the nebular phase (at the end of the plateau).

Our main results are summarized as follows:

- We confirm previous results showing that brighter SNe II have higher expansion velocities. Here we show that this finding is true for all SN II decline rates, and also extends to magnitudes measured at maximum and during the radioactive tail. These results are most easily explained through differences in explosion energy: more energetic explosions produce brighter and higher velocity SNe II. Additionally we find that more energetic (brighter and faster) events produce more ^{56}Ni.
- We highlight our different definition of the plateau

duration (Pd) in this work as compared with the literature: from the s_1–s_2 transition to the end of the plateau, and conclude that it is a more robust parameter connected to H-rich envelope mass. Indeed, we find that Pd shows much stronger correlations with other parameters than the traditionally used definition ($OPTd$ in our nomenclature). We conclude that Pd, s_3 and a/e are most directly affected by the hydrogen envelope mass at explosion epoch.

- While we have found many different trends and correlations between different spectral and photometric parameters of SNe II, hinting at underlying physical trends driving diversity (explosion energy, hydrogen envelope mass, ^{56}Ni mass), we conclude there is no one parameter dominating these trends.

- As expected, expansion velocities measured for different spectral lines correlate strongly with each other. However, velocities for different lines for individual SNe II are significantly offset, suggesting that they form at different regions at differing distances from the photosphere.

- Brighter SNe have higher velocities, smaller pEWs, shorter a/e, steeper declines and small Pd and $OPTd$ values.

C.P.G., S.G.G. acknowledge support by projects IC120009 "Millennium Institute of Astrophysics (MAS)" and P10-064-F "Millennium Center for Supernova Science" of the Iniciativa Cientfica Milenio del Ministerio Economa, Fomento y Turismo de Chile. C.P.G. acknowledges support from EU/FP7-ERC grant No. [615929]. M. D. S. is supported by the Danish Agency for Science and Technology and Innovation realized through a Sapere Aude Level 2 grant and by a research grant (13261) from the VILLUM FONDEN. We gratefully acknowledge support of the CSP by the NSF under grants AST0306969, AST0908886, AST0607438, and AST1008343. This research has made use of the NASA/IPAC Extragalactic Database (NED) which is operated by the Jet Propulsion Laboratory, California Institute of Technology, under contract with the National Aeronautics.

REFERENCES

Anderson, J. P., Dessart, L., Gutierrez, C. P., et al. 2014a, MNRAS, 441, 671
Anderson, J. P., et al. 2014b, ApJ, 786, 67
Anderson, J. P., Gutiérrez, C. P., Dessart, L., et al. 2016, A&A, 589, A110
Barbon, R., Ciatti, F., & Rosino, L. 1979, A&A, 72, 287
Bartunov, O. S., & Blinnikov, S. I. 1992, Soviet Astronomy Letters, 18, 43
Bersten, M. C. 2013, ArXiv e-prints
Blanco, V. M., Gregory, B., Hamuy, M., et al. 1987, ApJ, 320, 589
Chevalier, R. A. 1976, ApJ, 207, 872
Dessart, L., & Hillier, D. J. 2005, A&A, 437, 667
—. 2011, MNRAS, 410, 1739
Dessart, L., Hillier, D. J., & Audit, E. 2017, ArXiv e-prints
Dessart, L., Hillier, D. J., Waldman, R., & Livne, E. 2013a, MNRAS, 433, 1745
Dessart, L., Livne, E., & Waldman, R. 2010a, MNRAS, 408, 827
—. 2010b, MNRAS, 405, 2113
Dessart, L., Waldman, R., Livne, E., Hillier, D. J., & Blondin, S. 2013b, MNRAS, 428, 3227
Dessart, L., Gutierrez, C. P., Hamuy, M., et al. 2014, MNRAS, 440, 1856
Elias-Rosa, N., Van Dyk, S. D., Li, W., et al. 2010, ApJ, 714, L254
—. 2011, ApJ, 742, 6
Evans, J. D. 1996, Pacific Grove, CA: Brooks/Cole Publishing
Falk, S. W., & Arnett, W. D. 1977, ApJS, 33, 515
Faran, T., Poznanski, D., Filippenko, A. V., et al. 2014a, MNRAS, 445, 554
—. 2014b, MNRAS, 442, 844
Filippenko, A. V. 1997, ARA&A, 35, 309
Filippenko, A. V., Matheson, T., & Ho, L. C. 1993, ApJ, 415, L103
Galbany, L., Hamuy, M., Phillips, M. M., et al. 2016, AJ, 151, 33
González-Gaitán, S., Tominaga, N., Molina, J., et al. 2015, MNRAS, 451, 2212
Grassberg, E. K., Imshennik, V. S., & Nadyozhin, D. K. 1971, Ap&SS, 10, 28
Gutiérrez, C. P., et al. 2014, ApJ, 786, L15
Hamuy, M. 2003, ApJ, 582, 905
Hamuy, M., & Pinto, P. A. 2002, ApJ, 566, L63
Hamuy, M., Suntzeff, N. B., Gonzalez, R., & Martin, G. 1988, AJ, 95, 63
Hamuy, M., Maza, J., Pinto, P. A., et al. 2002, AJ, 124, 417
Inserra, C., Pastorello, A., Turatto, M., et al. 2013, A&A, 555, A142
Kasen, D., & Woosley, S. E. 2009, ApJ, 703, 2205
Kelly, B. C. 2007, ApJ, 665, 1489
Litvinova, I. I., & Nadezhin, D. K. 1983, Ap&SS, 89, 89
Maund, J. R., Fraser, M., Reilly, E., Ergon, M., & Mattila, S. 2015, MNRAS, 447, 3207
Maund, J. R., & Smartt, S. J. 2005, MNRAS, 360, 288
Menzies, J. W., Catchpole, R. M., van Vuuren, G., et al. 1987, MNRAS, 227, 39P
Minkowski, R. 1941, PASP, 53, 224
Moriya, T. J., Pruzhinskaya, M. V., Ergon, M., & Blinnikov, S. I. 2016, MNRAS, 455, 423
Moriya, T. J., Yoon, S.-C., Gräfener, G., & Blinnikov, S. I. 2017, MNRAS, 469, L108
Morozova, V., Piro, A. L., Renzo, M., & Ott, C. D. 2016, ApJ, 829, 109
Morozova, V., Piro, A. L., Renzo, M., et al. 2015, ApJ, 814, 63
Morozova, V., Piro, A. L., & Valenti, S. 2017, ApJ, 838, 28
Müller, T., Prieto, J. L., Pejcha, O., & Clocchiatti, A. 2017, ApJ, 841, 127
Nakar, E., Poznanski, D., & Katz, B. 2016, ApJ, 823, 127
Pastorello, A., Ramina, M., Zampieri, L., et al. 2003, ArXiv Astrophysics e-prints
Pastorello, A., Zampieri, L., Turatto, M., et al. 2004, MNRAS, 347, 74
Pastorello, A., Baron, E., Branch, D., et al. 2005, MNRAS, 360, 950
Pastorello, A., Pumo, M. L., Navasardyan, H., et al. 2012, A&A, 537, A141
Patat, F., Barbon, R., Cappellaro, E., & Turatto, M. 1994, A&A, 282, 731
Pejcha, O., & Prieto, J. L. 2015a, ApJ, 799, 215
—. 2015b, ApJ, 806, 225
Phillips, M. M., Heathcote, S. R., Hamuy, M., & Navarrete, M. 1988, AJ, 95, 1087
Popov, D. V. 1993, ApJ, 414, 712
Roy, R., Kumar, B., Benetti, S., et al. 2011, ApJ, 736, 76
Sanders, N. E., Soderberg, A. M., Gezari, S., et al. 2015, ApJ, 799, 208
Schlegel, E. M. 1990, MNRAS, 244, 269
—. 1996, AJ, 111, 1660
Smartt, S. J. 2015, Publications of the Astronomical Society of Australia, 32, e016
Smartt, S. J., Eldridge, J. J., Crockett, R. M., & Maund, J. R. 2009, MNRAS, 395, 1409
Smartt, S. J., Maund, J. R., Hendry, M. A., et al. 2004, Science, 303, 499
Spiro, S., Pastorello, A., Pumo, M. L., et al. 2014, MNRAS, 439, 2873

Suntzeff, N. B., Hamuy, M., Martin, G., Gomez, A., & Gonzalez, R. 1988, AJ, 96, 1864
Taddia, F., et al. 2013, A&A, 555, A10
Takáts, K., Pumo, M. L., Elias-Rosa, N., et al. 2014, MNRAS, 438, 368
Valenti, S., Howell, D. A., Stritzinger, M. D., et al. 2016, MNRAS, 459, 3939
Van Dyk, S. D., Li, W., & Filippenko, A. V. 2003, PASP, 115, 1289
Woosley, S. E., Hartmann, D., & Pinto, P. A. 1989, ApJ, 346, 395
Yaron, O., Perley, D. A., Gal-Yam, A., et al. 2017, Nature Physics, 13, 510
Young, T. R. 2004, ApJ, 617, 1233

Table 1 Photometric parameters

SN	Pd (days)	$OPTd$ (days)	Cd (days)	M_{max} (mag)	M_{end} (mag)	M_{tail} (mag)	s_1 (mag.100d^{-1})	s_2 (mag.100d^{-1})	s_3 (mag.100d^{-1})	^{56}Ni mass $M_\odot$	$\Delta(B\text{-}V)_{10,30}$
1986L	59.56 ± 0.71	93.74 ± 6.71	34.18 ± 3.08	-18.19 ± 0.20	-16.88 ± 0.20	-14.37 ± 0.20	3.26 ± 0.14	1.26 ± 0.03	···	>0.061	2.63 ± 0.42
1990K	···	···	···	···	···	···	···	2.39 ± 0.08	···	···	···
1991al	···	···	···	-17.51 ± 0.15	-17.03 ± 0.15	-14.71 ± 0.15	···	1.45 ± 0.04	1.26 ± 0.26	$0.067^{+0.016}_{-0.021}$	3.69 ± 0.24
1992af	···	47.03 ± 6.71	···	-17.33 ± 0.12	-17.20 ± 0.12	-15.06 ± 0.12	···	0.58 ± 0.03	1.07 ± 0.08	$0.079^{+0.018}_{-0.029}$	1.90 ± 0.83
1992ba	···	106.97 ± 8.54	···	-15.34 ± 0.80	-14.75 ± 0.80	-12.34 ± 0.80	···	0.72 ± 0.02	0.86 ± 0.07	$0.011^{+0.006}_{-0.015}$	2.80 ± 0.21
1993K	···	···	···	-17.92 ± 0.23	-17.24 ± 0.23	···	···	2.36 ± 0.08	···	···	1.82 ± 0.09
1993S	···	···	···	-17.52 ± 0.07	-16.29 ± 0.07	···	···	2.34 ± 0.04	···	···	3.63 ± 0.51
1999br	···	···	···	-13.77 ± 0.40	-13.56 ± 0.40	···	···	0.14 ± 0.02	···	>0.002	3.58 ± 0.39
1999ca	40.54 ± 0.92	79.48 ± 7.62	38.94 ± 7.06	-17.48 ± 0.21	-16.60 ± 0.21	-13.78 ± 0.21	3.49 ± 0.16	1.65 ± 0.06	1.74 ± 0.33	>0.047	···
1999cr	43.55 ± 1.68	79.06 ± 7.62	35.51 ± 4.34	-16.90 ± 0.10	-16.23 ± 0.10	···	1.78 ± 0.09	0.49 ± 0.08	···	···	1.77 ± 0.38
1999em	67.04 ± 2.12	96.04 ± 5.83	29.00 ± 5.43	-16.76 ± 0.07	-16.37 ± 0.07	-13.93 ± 0.07	0.86 ± 0.11	0.30 ± 0.02	0.88 ± 0.05	$0.050^{+0.008}_{-0.009}$	3.07 ± 0.23
S0210	···	93.57 ± 9.49	···	-16.21 ± 0.04	-15.90 ± 0.04	···	···	2.37 ± 0.07	···	···	···
2002fa	···	68.289 ± 7.62	···	-16.95 ± 0.04	-16.65 ± 0.04	···	···	1.56 ± 0.11	···	>0.066	···
2002gd	···	···	35.00 ± 4.09	-15.43 ± 0.28	-14.85 ± 0.28	···	1.87 ± 0.09	0.15 ± 0.04	···	···	3.21 ± 0.28
2002gw	···	88.33 ± 5.83	···	-15.76 ± 0.23	-15.48 ± 0.23	-13.07 ± 0.23	···	0.22 ± 0.03	0.75 ± 0.09	$0.012^{+0.003}_{-0.004}$	2.55 ± 0.20
2002hj	···	90.24 ± 7.62	···	-16.91 ± 0.10	-16.03 ± 0.10	-13.59 ± 0.10	···	1.57 ± 0.05	1.41 ± 0.01	>0.026	···
2002hx	···	68.03 ± 9.49	···	-17.00 ± 0.07	-16.36 ± 0.07	-14.60 ± 0.07	···	1.51 ± 0.03	1.24 ± 0.04	$0.053^{+0.016}_{-0.023}$	2.26 ± 0.32
2002ig	···	···	···	-17.66 ± 0.03	-16.76 ± 0.03	···	···	2.20 ± 0.12	···	···	2.42 ± 0.66
2003B	···	86.19 ± 11.40	···	-15.36 ± 0.28	-15.11 ± 0.28	-12.77 ± 0.28	···	0.65 ± 0.03	1.07 ± 0.03	$0.017^{+0.006}_{-0.009}$	···
2003bl	···	95.81 ± 4.24	···	-15.35 ± 0.14	-15.01 ± 0.14	···	···	0.35 ± 0.02	···	···	2.83 ± 0.46
2003bn	62.96 ± 10.51	92.97 ± 4.24	30.01 ± 10.93	-16.80 ± 0.16	-16.34 ± 0.16	-13.72 ± 0.16	1.38 ± 0.9	0.32 ± 0.03	···	>0.038	2.94 ± 0.25
2003ci	···	92.53 ± 8.54	···	-16.83 ± 0.07	-15.70 ± 0.07	···	···	1.91 ± 0.04	···	···	···
2003cn	48.86 ± 3.99	69.8 ± 5.00	20.94 ± 5.65	-16.26 ± 0.11	-15.61 ± 0.11	···	2.7 ± 1.14	1.34 ± 0.04	···	···	2.73 ± 0.45
2003cx	···	90.82 ± 5.83	···	-16.79 ± 0.06	-16.38 ± 0.06	-14.32 ± 0.06	···	0.61 ± 0.04	···	>0.051	1.95 ± 0.65
2003E	···	101.42 ± 7.62	···	-15.70 ± 0.15	-15.48 ± 0.15	···	···	-0.10 ± 0.03	···	···	1.49 ± 0.25
2003ef	···	92.93 ± 9.49	···	-16.72 ± 0.14	-16.15 ± 0.14	···	···	0.78 ± 0.02	···	···	2.76 ± 0.39
2003eg	···	···	30.87 ± 5.04	-17.81 ± 0.13	-14.57 ± 0.13	···	6.75 ± 0.18	1.73 ± 0.13	···	···	1.35 ± 0.18
2003ej	···	68.97 ± 5.83	···	-17.66 ± 0.12	-15.66 ± 0.12	···	···	3.29 ± 0.04	···	···	2.95 ± 0.29
2003fb	···	88.27 ± 6.71	···	-15.56 ± 0.12	-15.25 ± 0.12	-13.10 ± 0.12	···	0.46 ± 0.06	1.61 ± 0.39	>0.017	···
2003gd	···	···	···	···	-15.97 ± 0.40	-12.58 ± 0.40	···	2.22 ± 0.05	1.03 ± 0.04	$0.012^{+0.006}_{-0.012}$	···
2003hd	···	84.39 ± 5.83	···	-17.29 ± 0.06	-16.72 ± 0.06	-13.85 ± 0.06	···	0.93 ± 0.04	0.72 ± 0.68	$0.029^{+0.007}_{-0.009}$	2.80 ± 0.21
2003hg	63.98 ± 1.67	108.5 ± 5.83	44.52 ± 5.27	-16.38 ± 0.16	-15.50 ± 0.16	···	1.35 ± 0.05	0.52 ± 0.04	···	···	3.01 ± 0.47
2003hk	58.96 ± 2.34	87.00 ± 5.00	28.04 ± 4.63	-17.02 ± 0.10	-16.36 ± 0.10	-13.14 ± 0.10	3.09 ± 0.20	1.61 ± 0.06	0.40 ± 0.66	>0.017	···
2003hl	···	108.92 ± 5.83	···	-15.91 ± 0.30	-15.23 ± 0.30	···	···	0.76 ± 0.01	···	···	2.92 ± 0.31
2003hn	58.34 ± 1.55	90.1 ± 10.44	31.76 ± 10.12	-16.74 ± 0.10	-15.96 ± 0.10	-13.27 ± 0.10	5.69 ± 0.27	2.52 ± 0.07	1.08 ± 0.05	$0.035^{+0.008}_{-0.011}$	2.88 ± 0.29
2003ho	···	···	···	···	-14.75 ± 0.16	-12.00 ± 0.16	···	2.25 ± 0.11	1.69 ± 0.10	>0.005	···
2003ib	···	···	···	-17.10 ± 0.09	-16.09 ± 0.09	···	···	1.64 ± 0.03	···	···	1.16 ± 0.22
2003ip	···	80.74 ± 5.00	···	-17.75 ± 0.13	-16.65 ± 0.13	···	···	2.03 ± 0.03	···	···	2.31 ± 0.25
2003iq	···	84.91 ± 3.61	···	-16.69 ± 0.30	-16.18 ± 0.30	···	···	0.72 ± 0.01	···	···	2.42 ± 0.28
2003T	···	90.59 ± 10.44	···	-16.54 ± 0.08	-16.03 ± 0.08	-13.67 ± 0.08	···	0.69 ± 0.02	2.02 ± 0.14	>0.030	2.74 ± 0.82
2004ej	···	97.14 ± 8.54	···	-16.62 ± 0.21	-16.13 ± 0.21	-12.92 ± 0.21	···	1.04 ± 0.04	0.89 ± 0.13	$0.019^{+0.005}_{-0.007}$	···
2004er	57.27 ± 1.66	120.12 ± 5.00	62.85 ± 2.6	-16.74 ± 0.16	-15.67 ± 0.16	···	1.08 ± 0.02	0.52 ± 0.02	···	···	2.13 ± 1.53
2004fb	···	···	···	-16.19 ± 0.11	-15.46 ± 0.11	···	···	1.26 ± 0.07	···	···	···
2004fc	68.06 ± 2.68	106.06 ± 3.16	38.00 ± 2.86	-16.21 ± 0.31	-15.41 ± 0.31	···	1.13 ± 0.03	0.50 ± 0.05	···	···	2.92 ± 0.20
2004fx	···	68.41 ± 5.00	···	-15.58 ± 0.24	-15.33 ± 0.24	-12.87 ± 0.24	···	0.25 ± 0.02	0.93 ± 0.08	$0.014^{+0.004}_{-0.006}$	1.52 ± 0.20
2005af	···	107.01 ± 15.30	···	···	-14.94 ± 0.36	-13.41 ± 0.36	···	0.40 ± 0.05	1.25 ± 0.03	$0.026^{+0.012}_{-0.021}$	···
2005an	36.02 ± 0.63	74.67 ± 5.00	38.65 ± 6.03	-17.07 ± 0.18	-15.89 ± 0.18	···	3.21 ± 0.05	1.85 ± 0.05	···	···	2.89 ± 0.08
2005dk	38.97 ± 1.47	82.24 ± 6.71	43.27 ± 6.18	-17.52 ± 0.14	-16.74 ± 0.14	···	2.25 ± 0.09	1.10 ± 0.07	···	···	···
2005dn	45.82 ± 3.31	78.72 ± 6.71	32.9 ± 6.85	-17.01 ± 0.24	-16.38 ± 0.24	···	2.00 ± 0.23	1.48 ± 0.04	···	···	···
2005dt	···	112.9 ± 9.49	···	-16.39 ± 0.09	-15.84 ± 0.09	···	···	0.58 ± 0.06	···	···	···
2005dx	···	89.98 ± 7.62	···	-16.05 ± 0.08	-15.24 ± 0.08	-12.12 ± 0.08	···	1.26 ± 0.05	···	>0.007	3.21 ± 0.31
2005dz	32.40 ± 2.84	81.86 ± 5.00	49.46 ± 4.91	-16.57 ± 0.12	-15.97 ± 0.12	-13.42 ± 0.12	1.09 ± 0.03	0.36 ± 0.10	···	>0.021	2.28 ± 0.25

2005J	53.01 ± 1.93	97.01 ± 7.62	44.00 ± 7.26	-17.28 ± 0.14	-16.35 ± 0.14	···	1.51 ± 0.03	1.04 ± 0.02	···	···	2.93 ± 0.17
2005lw	···	107.25 ± 10.44	···	-17.07 ± 0.08	-15.47 ± 0.08	···	···	2.04 ± 0.04	···	···	2.86 ± 0.70
2005Z	···	78.88 ± 6.71	···	-17.17 ± 0.11	-16.17 ± 0.11	···	···	1.76 ± 0.01	···	···	3.04 ± 0.29
2006ai	38.28 ± 0.46	63.26 ± 5.83	24.98 ± 5.02	-18.06 ± 0.14	-17.03 ± 0.14	-14.53 ± 0.14	4.61 ± 0.10	2.05 ± 0.04	1.78 ± 0.24	>0.050	2.02 ± 0.15
2006be	43.81 ± 1.32	76.2 ± 6.71	32.39 ± 9.10	-16.47 ± 0.29	-16.08 ± 0.29	···	1.19 ± 0.08	0.63 ± 0.02	···	···	3.04 ± 0.11
2006bl	···	···	17.3 ± 11.16	-18.23 ± 0.07	-16.52 ± 0.07	···	3.05 ± 0.54	2.41 ± 0.06	···	···	2.15 ± 0.38
2006ee	59.04 ± 2.95	85.15 ± 5.00	26.11 ± 4.97	-16.28 ± 0.15	-16.04 ± 0.15	···	0.98 ± 0.29	0.17 ± 0.03	···	···	2.45 ± 0.19
2006it	···	···	···	-16.20 ± 0.15	-15.97 ± 0.15	···	···	1.14 ± 0.10	···	···	3.98 ± 0.14
2006iw	···	···	···	-16.89 ± 0.07	-16.18 ± 0.07	···	···	1.00 ± 0.03	···	···	2.24 ± 0.67
2006ms	···	···	32.83 ± 6.62	-16.18 ± 0.15	-15.93 ± 0.15	···	1.65 ± 0.2	-0.05 ± 0.45	···	>0.056	4.12 ± 0.12
2006qr	···	96.85 ± 7.62	···	-15.99 ± 0.14	-14.24 ± 0.14	···	···	1.40 ± 0.02	···	···	2.88 ± 0.45
2006Y	24.69 ± 0.63	47.49 ± 5.00	22.8 ± 4.05	-17.97 ± 0.06	-16.98 ± 0.06	-14.26 ± 0.06	5.84 ± 0.13	2.11 ± 0.18	4.75 ± 0.34	>0.034	1.52 ± 0.25
2007aa	···	···	···	-16.32 ± 0.27	-16.32 ± 0.27	···	···	-0.05 ± 0.02	···	···	···
2007ab	···	71.66 ± 10.44	···	-16.98 ± 0.09	-16.55 ± 0.09	-14.22 ± 0.09	···	3.18 ± 0.06	2.31 ± 0.22	>0.040	···
2007av	···	···	···	-16.27 ± 0.22	-15.60 ± 0.22	···	···	0.92 ± 0.01	···	>0.015	2.21 ± 0.13
2007bf	···	···	···	···	···	···	···	···	···	···	···
2007hm	···	···	···	-16.47 ± 0.09	-16.00 ± 0.09	···	···	1.52 ± 0.04	···	>0.045	1.43 ± 0.28
2007il	68.68 ± 2.43	103.4 ± 5.00	34.72 ± 4.68	-16.78 ± 0.11	-16.59 ± 0.11	···	1.06 ± 0.34	0.12 ± 0.04	···	···	2.21 ± 0.12
2007it	···	···	13.95 ± 2.64	-17.55 ± 0.50	···	-14.83 ± 0.50	3.55 ± 1.06	1.33 ± 0.14	1.00 ± 0.01	$0.072^{+0.031}_{-0.054}$	2.67 ± 0.10
2007ld	···	···	···	-17.30 ± 0.09	-16.53 ± 0.09	···	···	2.62 ± 0.04	···	···	2.13 ± 0.50
2007oc	42.78 ± 0.59	71.62 ± 5.83	28.84 ± 3.06	-16.68 ± 0.15	-16.02 ± 0.15	···	2.87 ± 0.10	1.78 ± 0.01	···	···	···
2007od	···	···	19.61 ± 5.06	-17.87 ± 0.80	-16.81 ± 0.80	···	2.56 ± 0.10	1.50 ± 0.02	···	···	2.37 ± 0.12
2007P	61.34 ± 1.19	88.34 ± 5.83	27.00 ± 5.14	-17.96 ± 0.05	-16.75 ± 0.05	···	3.80 ± 0.16	1.40 ± 0.12	···	···	2.26 ± 0.38
2007sq	44.66 ± 2.39	87.66 ± 5.00	43.00 ± 6.46	-15.33 ± 0.13	-14.52 ± 0.13	···	2.52 ± 0.37	1.29 ± 0.08	···	···	···
2007U	···	···	···	-17.87 ± 0.08	-16.78 ± 0.08	···	···	2.27 ± 0.04	···	···	2.63 ± 0.35
2007W	56.71 ± 2.57	83.59 ± 7.62	26.88 ± 7.46	-15.80 ± 0.20	-15.34 ± 0.20	···	0.83 ± 0.27	0.00 ± 0.04	···	···	2.39 ± 0.28
2007X	53.92 ± 1.03	98.06 ± 5.83	44.14 ± 5.14	-17.84 ± 0.21	-16.70 ± 0.21	···	2.52 ± 0.07	1.37 ± 0.03	···	···	3.55 ± 0.15
2008ag	···	105.3 ± 6.71	···	-16.96 ± 0.15	-16.66 ± 0.15	···	···	0.12 ± 0.01	···	···	···
2008aw	37.91 ± 0.91	75.82 ± 10.44	37.91 ± 10.04	-17.71 ± 0.19	-16.60 ± 0.19	-14.04 ± 0.19	3.27 ± 0.08	2.10 ± 0.05	1.97 ± 0.09	>0.050	2.85 ± 0.16
2008bh	···	···	20.68 ± 5.34	-16.06 ± 0.14	-15.11 ± 0.14	···	2.69 ± 0.23	1.20 ± 0.04	···	···	2.17 ± 0.38
2008bk	···	107.22 ± 6.71	···	-14.86 ± 0.05	-14.59 ± 0.05	-11.98 ± 0.05	···	0.26 ± 0.01	1.18 ± 0.02	$0.007^{+0.001}_{-0.001}$	···
2008bm	···	87.04 ± 26.17	···	-18.12 ± 0.07	-16.32 ± 0.07	-12.67 ± 0.07	···	2.50 ± 0.03	···	>0.014	···
2008bp	···	58.57 ± 9.49	···	-14.00 ± 0.21	-13.13 ± 0.21	···	···	2.79 ± 0.13	···	···	1.79 ± 0.42
2008br	···	···	···	-15.30 ± 0.20	-14.94 ± 0.20	···	···	0.38 ± 0.04	···	>0.026	2.19 ± 0.22
2008bu	···	44.73 ± 7.62	···	-17.14 ± 0.10	-16.74 ± 0.10	-13.71 ± 0.10	···	2.37 ± 0.18	2.69 ± 0.52	>0.020	2.98 ± 0.37
2008ga	···	73.14 ± 5.00	···	-16.45 ± 0.14	-16.20 ± 0.14	···	···	1.10 ± 0.07	···	···	···
2008gi	···	···	···	-17.31 ± 0.09	-15.86 ± 0.09	···	···	2.63 ± 0.11	···	···	2.55 ± 1.35
2008gr	···	···	9.00 ± 6.17	-17.95 ± 0.10	-16.43 ± 0.10	···	2.22 ± 0.13	1.61 ± 0.03	···	···	2.46 ± 0.11
2008H	···	···	···	···	···	···	···	···	···	···	···
2008hg	···	···	···	-15.43 ± 0.12	-15.59 ± 0.12	···	···	-0.35 ± 0.08	···	···	3.25 ± 0.32
2008ho	···	···	···	-15.11 ± 0.23	-15.03 ± 0.23	···	···	0.32 ± 0.07	···	···	2.39 ± 0.19
2008if	51.04 ± 0.29	75.85 ± 5.83	24.81 ± 5.01	-17.94 ± 0.17	-16.79 ± 0.17	-14.46 ± 0.17	4.15 ± 0.07	1.99 ± 0.02	···	>0.063	1.76 ± 0.22
2008il	···	···	···	-16.61 ± 0.11	-16.22 ± 0.11	···	···	0.71 ± 0.05	···	···	2.39 ± 0.15
2008in	···	89.64 ± 6.71	···	-15.40 ± 0.47	-14.79 ± 0.47	···	···	0.91 ± 0.01	···	···	3.01 ± 0.13
2008K	···	89.32 ± 5.00	···	-17.45 ± 0.08	-16.04 ± 0.08	-13.40 ± 0.08	···	2.66 ± 0.02	2.07 ± 0.26	>0.013	2.61 ± 0.84
2008M	58.27 ± 0.27	75.35 ± 9.49	17.08 ± 9.00	-16.75 ± 0.28	-16.17 ± 0.28	-13.41 ± 0.28	5.15 ± 0.27	0.94 ± 0.02	1.18 ± 0.26	$0.020^{+0.007}_{-0.010}$	1.79 ± 0.18
2008W	···	85.84 ± 6.71	···	-16.60 ± 0.11	-16.05 ± 0.11	···	···	1.10 ± 0.04	···	···	···
2009aj	···	···	···	-18.07 ± 0.20	-16.85 ± 0.20	···	···	···	···	···	···
2009ao	···	41.68 ± 5.00	···	-15.79 ± 0.20	-15.78 ± 0.20	···	···	-0.01 ± 0.12	···	···	1.75 ± 0.29
2009au	···	···	···	-16.34 ± 0.21	-14.69 ± 0.21	···	···	3.03 ± 0.02	···	···	2.04 ± 0.31
2009bu	···	···	37.35 ± 8.23	-16.05 ± 0.19	-15.87 ± 0.19	···	0.91 ± 0.14	0.13 ± 0.04	···	···	···
2009bz	···	···	···	-16.46 ± 0.19	-16.26 ± 0.19	···	···	0.36 ± 0.03	···	···	2.14 ± 0.15
2009N	66.73 ± 0.48	89.79 ± 5.83	23.06 ± 5.02	-15.25 ± 0.40	-14.90 ± 0.40	···	2.00 ± 0.29	0.22 ± 0.01	···	···	3.50 ± 0.06

Same as Anderson et al. (2014b): In the first column we list the SN name. Columns 2, 3 and 4 shows the *Pd*, *OPTd* and *Cd*. In columns 5, 6 and 7 we list the absolute magnitudes of M_{max}, M_{end} and M_{tail} respectively. These are followed by the decline rates: s_1, s_2 and s_3, in columns 8, 9 and 10 respectively. In column 11 we present the derived ^{56}Ni masses (or lower limits), while in column 12 the color gradient is shown.

As it is explained in Section 3, the *Pd*, s_1, s2 show differences with respect to Anderson et al. (2014b).

Table 2
Average of correlations

Parameter	Average at 30 days	Average at 50 days	Average at 80 days
Pd	0.370	0.410	0.425
OPTd	0.305	0.316	0.342
Cd	0.225	0.228	0.233
M_{max}	0.392	0.417	0.375
M_{end}	0.325	0.345	0.343
M_{tail}	0.406	0.423	0.456
s_1	0.355	0.391	0.344
s_2	0.304	0.348	0.325
s_3	0.334	0.374	0.363
^{56}Ni	0.449	0.520	0.550
$\Delta C_(10-30)$	0.208	0.219	0.213
V(H_α)	0.361	0.468	0.452
V(H_β)	0.416	0.479	0.441
V(Fe II 5018)	0.380	0.450	0.325
V(Fe II 5169)	0.415	0.477	0.393
V(Na I D)	0.450	0.519	0.480
pEW(H_α)$_a$	0.279	0.270	0.287
pEW(H_α)$_e$	0.138	0.362	0.427
pEW(Fe II 5018)	0.329	0.339	0.218
pEW(Fe II 5169)	0.167	0.209	0.189
pEW(Na I D)	0.238	0.242	0.354
a/e	0.269	0.328	0.316
Δvel(H_α - Fe II 5018)	0.303	0.321	0.438
Δvel(Na I D - Fe II 5018)	0.403	0.426	0.419
$\Delta v(H_\beta)$	0.248	0.228	0.207

Average of the correlations at 30, 50 and 80 days since explosion presented for 11 photometric parameters and 14 spectroscopic ones. In the first column the SN II parameter is listed (described in 3), while in the second, three and four column are the average.

Table 3 Velocity values at 50 days from explosion

SN	$vel(H_\alpha)$ (km s^{-1})	$vel(H_\alpha)$ (km s^{-1})	$vel(H_\beta)$ (km s^{-1})	vel(Fe II λ4924) (km s^{-1})	vel(Fe II λ5018) (km s^{-1})	vel(Fe II λ5169) (km s^{-1})	vel(Fe II /Sc II) (km s^{-1})	vel(Sc II Mult.) (km s^{-1})	vel(Na I D) (km s^{-1})	vel(Ba II) (km s^{-1})	vel(ScII) (km s^{-1})	vel(O I) (km s^{-1})
1986L	7707 ± 710	6204 ± 476	6722 ± 434	4946 ± 245	4311 ± 672	4406 ± 411	4778 ± 456	4316 ± 336	5512 ± 486	···	···	···
1990K	7841 ± 432	6958 ± 426	6563 ± 381	···	4440 ± 298	3942 ± 204	4886 ± 450	4604 ± 239	6363 ± 391	4468 ± 312	4139 ± 238	···
1991al	8897 ± 496	7950 ± 615	7789 ± 634	4921 ± 244	4790 ± 588	4982 ± 548	5256 ± 261	4575 ± 227	7835 ± 876	5696 ± 282	4149 ± 206	···
1992af	···	···	···	···	···	···	···	···	···	···	···	···
1992ba	6276 ± 665	4559 ± 439	5100 ± 374	3160 ± 157	3388 ± 487	3464 ± 483	3479 ± 173	3322 ± 165	4325 ± 847	3042 ± 151	3060 ± 152	···
1993K	7099 ± 551	7151 ± 358	6326 ± 444	4903 ± 269	3536 ± 490	4390 ± 218	4479 ± 222	3767 ± 270	5488 ± 520	3998 ± 199	4053 ± 420	4500 ± 466
1993S	7800 ± 630	6132 ± 620	6886 ± 670	3269 ± 340	4822 ± 470	4943 ± 300	···	···	6071 ± 620	···	···	···
1999br	3611 ± 588	3082 ± 265	3191 ± 243	1511 ± 258	1753 ± 223	1746 ± 305	2101 ± 272	1527 ± 443	1519 ± 759	1229 ± 61	1891 ± 94	1100 ± 100
1999ca	7375 ± 348	7039 ± 364	6840 ± 338	···	5618 ± 278	5191 ± 257	6103 ± 302	5727 ± 284	6825 ± 337	5833 ± 289	5043 ± 250	···
1999cr	5960 ± 361	5477 ± 323	4932 ± 478	···	3495 ± 195	3655 ± 212	···	3909 ± 194	4504 ± 224	···	···	···
1999em	6025 ± 622	5591 ± 595	5709 ± 626	3768 ± 187	3337 ± 394	3464 ± 365	3383 ± 168	2992 ± 149	3722 ± 451	3048 ± 152	3107 ± 154	···
S0210	7955 ± 492	8197 ± 762	7050 ± 619	···	6846 ± 424	4998 ± 326	6276 ± 311	5374 ± 550	6810 ± 455	···	···	···
2002fa	7649 ± 649	6184 ± 435	6359 ± 410	3567 ± 268	3832 ± 337	4133 ± 260	4163 ± 207	3603 ± 179	5741 ± 663	···	···	···
2002gd	4138 ± 563	3717 ± 266	3414 ± 703	2257 ± 196	2730 ± 204	2448 ± 236	3165 ± 297	3005 ± 409	3406 ± 273	2105 ± 177	2414 ± 325	1870 ± 200
2002gw	6674 ± 474	5454 ± 487	5299 ± 518	3253 ± 329	3295 ± 494	3623 ± 357	3221 ± 345	3233 ± 247	3889 ± 304	3036 ± 211	2976 ± 185	3120 ± 325
2002hj	7933 ± 661	6540 ± 532	6447 ± 451	3432 ± 579	3787 ± 338	4192 ± 405	4645 ± 230	3592 ± 220	5239 ± 345	···	···	4080 ± 420
2002hx	8070 ± 434	5722 ± 504	6455 ± 554	3255 ± 337	3506 ± 215	3806 ± 284	3021 ± 157	3623 ± 200	5408 ± 477	2532 ± 160	3213 ± 302	···
2002ig	···	···	···	···	···	···	···	···	···	···	···	···
2003B	6256 ± 339	4604 ± 622	5524 ± 478	3204 ± 575	3458 ± 297	3509 ± 251	3643 ± 260	3523 ± 307	4051 ± 228	3343 ± 265	3121 ± 188	2970 ± 270
2003bl	3958 ± 481	3679 ± 435	3849 ± 326	4297 ± 255	2342 ± 213	2093 ± 190	2451 ± 263	2456 ± 207	2712 ± 582	2780 ± 426	2265 ± 184	···
2003bn	6892 ± 638	5887 ± 545	5688 ± 471	3639 ± 265	3611 ± 607	3612 ± 530	3457 ± 302	3254 ± 327	4077 ± 397	3296 ± 300	3134 ± 178	3000 ± 280
2003ci	7219 ± 280	5648 ± 357	5916 ± 293	3007 ± 150	3832 ± 190	3677 ± 183	4761 ± 236	4449 ± 483	5907 ± 292	3142 ± 156	4254 ± 211	···
2003cn	5409 ± 293	4223 ± 501	4521 ± 946	2399 ± 119	2778 ± 138	2699 ± 197	2962 ± 147	2533 ± 126	3836 ± 695	2817 ± 140	2980 ± 148	···
2003cx	9001 ± 870	5960 ± 600	7038 ± 720	4753 ± 460	4130 ± 400	4788 ± 420	···	···	5993 ± 610	···	···	···
2003E	···	···	···	···	···	···	···	···	···	···	···	···
2003ef	7703 ± 367	6416 ± 610	4261 ± 494	3930 ± 364	4121 ± 534	4116 ± 516	4044 ± 575	3738 ± 395	4316 ± 484	3582 ± 299	3638 ± 181	3750 ± 390
2003eg	8560 ± 725	7619 ± 675	6705 ± 418	···	4669 ± 405	4727 ± 456	4168 ± 207	4235 ± 210	6993 ± 468	3100 ± 320	3390 ± 410	···
2003ej	6897 ± 630	9181 ± 1000	5968 ± 600	···	4998 ± 480	4381 ± 405	···	···	6244 ± 600	···	···	···
2003fb	7583 ± 561	6132 ± 625	5840 ± 854	3906 ± 754	4033 ± 738	3819 ± 722	3996 ± 704	3516 ± 677	4749 ± 668	4319 ± 649	3430 ± 627	···
2003gd	···	···	···	···	···	···	···	···	···	···	···	···
2003hd	7850 ± 519	6809 ± 539	5960 ± 717	3864 ± 192	3956 ± 260	4025 ± 289	3779 ± 188	3393 ± 169	4725 ± 234	···	···	···
2003hg	···	···	···	···	···	···	···	···	···	···	···	4090 ± 420
2003hk	6622 ± 349	7062 ± 328	5682 ± 281	4053 ± 201	4144 ± 206	4161 ± 207	···	···	5767 ± 286	···	···	···
2003hl	6579 ± 738	5623 ± 462	4550 ± 439	3961 ± 382	3899 ± 287	3819 ± 402	3787 ± 329	3783 ± 283	4527 ± 318	3276 ± 252	3501 ± 244	3570 ± 368
2003hn	7016 ± 387	6594 ± 462	5336 ± 442	3455 ± 281	3425 ± 249	3484 ± 379	3466 ± 286	3148 ± 293	4470 ± 339	3596 ± 189	3039 ± 375	3480 ± 360
2003ho	8312 ± 755	7459 ± 520	6102 ± 302	3463 ± 172	3739 ± 186	3989 ± 198	4309 ± 214	3969 ± 197	5010 ± 248	···	···	3970 ± 410
2003ib	···	···	···	···	···	···	···	···	···	···	···	···
2003ip	8629 ± 486	8059 ± 533	6813 ± 388	···	5391 ± 341	4536 ± 309	5773 ± 286	5058 ± 251	6501 ± 413	4858 ± 241	5337 ± 264	6100 ± 600
2003iq	7483 ± 741	5953 ± 386	5483 ± 350	4254 ± 211	4213 ± 225	4329 ± 216	4171 ± 207	3935 ± 195	5123 ± 360	3743 ± 186	3920 ± 195	3950 ± 330
2003T	6954 ± 403	5994 ± 634	4039 ± 226	3967 ± 341	3807 ± 218	3896 ± 276	3777 ± 190	3390 ± 222	3996 ± 292	4223 ± 257	4039 ± 240	···
2004ej	635 ± 501	5522 ± 429	5389 ± 600	3535 ± 505	3440 ± 307	3301 ± 221	3556 ± 536	3291 ± 319	4005 ± 326	2880 ± 191	3178 ± 223	3380 ± 350
2004er	965 ± 582	8323 ± 549	7878 ± 600	6040 ± 427	5396 ± 386	5219 ± 436	5501 ± 311	3372 ± 470	5771 ± 506	5284 ± 634	5306 ± 475	5065 ± 520
2004fb	769 ± 636	6678 ± 444	5884 ± 435	3926 ± 283	4228 ± 425	4178 ± 300	4368 ± 217	3750 ± 186	4798 ± 340	5254 ± 261	3805 ± 410	···
2004fc	633 ± 645	5639 ± 976	4056 ± 329	3690 ± 236	3675 ± 291	3581 ± 256	3760 ± 270	3591 ± 261	4194 ± 541	3195 ± 229	3386 ± 266	3319 ± 325
2004fx	572 ± 525	4856 ± 446	4194 ± 318	2385 ± 206	2700 ± 209	2786 ± 401	3002 ± 177	3386 ± 168	2884 ± 389	3180 ± 158	2459 ± 133	2300 ± 210
2005af	···	···	···	···	···	···	···	···	···	···	···	···
2005an	7656 ± 888	8325 ± 494	5346 ± 1497	4356 ± 219	4333 ± 325	4011 ± 303	4753 ± 289	4551 ± 293	4738 ± 560	···	···	4580 ± 470

2005dk	7926 ± 531	6887 ± 470	6883 ± 359	4541 ± 312	4535 ± 289	4603 ± 306	4418 ± 311	3937 ± 329	6317 ± 709	5112 ± 457	4039 ± 256	4420 ± 420
2005dn	9500 ± 672	8420 ± 576	7613 ± 484	2360 ± 118	5750 ± 1511	4712 ± 434	···	4857 ± 241	6518 ± 627	···	···	···
2005dt	···	···	···	···	···	···	···	···	···	···	···	···
2005dx	···	···	···	···	···	···	···	···	···	···	···	···
2005dz	7591 ± 595	6182 ± 434	5934 ± 430	925 ± 88	3927 ± 499	4101 ± 310	···	···	7397 ± 735	···	···	···
2005J	8434 ± 755	6353 ± 668	6380 ± 404	4235 ± 273	4129 ± 406	4224 ± 437	4151 ± 402	4190 ± 265	4994 ± 386	4097 ± 297	4581 ± 272	4500 ± 460
2005lw	···	···	···	···	···	···	···	···	···	···	···	···
2005Z	9479 ± 661	8538 ± 582	7879 ± 843	5673 ± 281	5646 ± 384	5196 ± 411	5633 ± 489	5435 ± 359	7375 ± 560	6432 ± 655	4671 ± 480	6040 ± 640
2006ai	7480 ± 821	6949 ± 559	6301 ± 560	4135 ± 353	4424 ± 427	4623 ± 340	4396 ± 258	3379 ± 526	6184 ± 434	···	···	6750 ± 710
2006be	7441 ± 474	6360 ± 625	5868 ± 755	3760 ± 742	3682 ± 738	3690 ± 722	3870 ± 694	3305 ± 677	4431 ± 668	4921 ± 620	···	···
2006bl	···	···	···	···	···	···	···	···	···	···	···	···
2006ee	5209 ± 426	5370 ± 675	3020 ± 619	3213 ± 254	3125 ± 194	3024 ± 255	3101 ± 299	2708 ± 316	3239 ± 267	2734 ± 262	2738 ± 202	···
2006it	···	···	···	···	···	···	···	···	···	···	···	···
2006iw	7373 ± 671	6104 ± 566	5337 ± 694	4352 ± 687	4127 ± 678	4148 ± 722	3790 ± 688	3352 ± 682	5074 ± 724	···	···	···
2006ms	···	···	···	···	···	···	···	···	···	···	···	···
2006qr	6501 ± 419	5558 ± 487	5103 ± 285	3166 ± 872	3593 ± 221	3643 ± 200	3780 ± 188	3529 ± 175	4844 ± 554	3795 ± 188	2932 ± 146	···
2006Y	9007 ± 619	7770 ± 589	6958 ± 464	3748 ± 186	4946 ± 731	5076 ± 546	···	···	7004 ± 613	···	···	···
2007aa	5985 ± 539	5102 ± 550	4264 ± 374	3148 ± 398	3179 ± 378	3148 ± 396	3099 ± 324	2880 ± 266	3864 ± 321	2697 ± 187	2907 ± 267	2650 ± 300
2007ab	9768 ± 505	8495 ± 600	8205 ± 405	···	7140 ± 353	4776 ± 237	6957 ± 344	6418 ± 318	7285 ± 404	6743 ± 337	5949 ± 614	···
2007av	7234 ± 338	6065 ± 402	5366 ± 311	3664 ± 182	3874 ± 192	3847 ± 191	3847 ± 191	3714 ± 185	3957 ± 605	3662 ± 182	3452 ± 172	3240 ± 299
2007bf	5498 ± 580	3830 ± 410	4110 ± 420	···	···	···	···	···	···	···	···	···
2007hm	8237 ± 383	6197 ± 544	6404 ± 432	4289 ± 213	4039 ± 201	4403 ± 515	4835 ± 240	3341 ± 166	5278 ± 262	···	···	···
2007il	8022 ± 809	7390 ± 482	5916 ± 505	4220 ± 281	4100 ± 481	4282 ± 383	4017 ± 370	4493 ± 420	4798 ± 769	5544 ± 560	2709 ± 250	···
2007it	···	···	···	···	···	···	···	···	···	···	···	···
2007ld	7176 ± 700	11416 ± 990	6024 ± 580	···	3695 ± 350	3589 ± 350	···	···	5922 ± 600	···	···	···
2007oc	6749 ± 492	7072 ± 435	5239 ± 436	2274 ± 198	3281 ± 315	3694 ± 343	4188 ± 480	3859 ± 378	5019 ± 450	2887 ± 218	3266 ± 291	4700 ± 500
2007od	7171 ± 655	7163 ± 428	6698 ± 545	···	5188 ± 363	3863 ± 300	···	3876 ± 193	6202 ± 427	5100 ± 525	4846 ± 240	···
2007P	···	···	···	···	···	···	···	···	···	···	···	···
2007sq	8298 ± 943	8409 ± 437	7410 ± 366	5270 ± 390	5249 ± 260	5350 ± 265	4978 ± 247	4135 ± 205	5662 ± 280	···	···	44780 ± 430
2007U	8037 ± 837	7395 ± 516	6911 ± 721	···	5541 ± 274	5439 ± 550	5923 ± 293	5429 ± 269	6480 ± 340	···	···	···
2007W	4754 ± 935	4125 ± 558	3203 ± 269	2343 ± 182	2612 ± 337	2437 ± 454	2543 ± 156	2505 ± 164	2618 ± 186	2086 ± 104	2485 ± 124	2000 ± 195
2007X	8597 ± 675	8418 ± 537	6685 ± 601	···	5466 ± 383	4619 ± 762	6339 ± 399	5555 ± 354	6170 ± 708	5160 ± 427	5021 ± 496	5980 ± 610
2008ag	6906 ± 463	6284 ± 426	4583 ± 473	4045 ± 292	3951 ± 324	3939 ± 311	3862 ± 326	3521 ± 283	4215 ± 426	3223 ± 230	3499 ± 233	3460 ± 330
2008aw	8257 ± 621	7783 ± 911	6641 ± 530	4728 ± 376	4724 ± 526	4532 ± 654	5027 ± 458	4429 ± 372	6436 ± 478	4545 ± 394	4458 ± 271	···
2008bh	7824 ± 688	7263 ± 430	6297 ± 375	4236 ± 210	4339 ± 232	4189 ± 637	4327 ± 215	4180 ± 207	4683 ± 378	4466 ± 222	3990 ± 198	···
2008bk	4115 ± 390	3313 ± 707	2401 ± 224	1867 ± 133	2256 ± 153	2910 ± 460	2266 ± 276	2437 ± 310	2019 ± 171	1846 ± 137	1998 ± 180	1780 ± 194
2008bm	1765 ± 56	11118 ± 88	1385 ± 69	1559 ± 78	1649 ± 82	1277 ± 64	···	···	1762 ± 88	···	···	···
2008bp	6795 ± 710	8613 ± 830	7497 ± 700	···	···	···	···	···	···	···	···	···
2008br	4070 ± 491	3682 ± 258	2484 ± 169	1665 ± 178	1832 ± 142	1633 ± 218	2161 ± 108	2547 ± 127	1922 ± 96	1386 ± 69	1670 ± 83	1420 ± 180
2008bu	···	···	···	···	···	···	···	···	···	···	···	···
2008ga	7313 ± 589	6400 ± 653	5357 ± 768	3307 ± 754	3390 ± 732	3253 ± 757	4665 ± 694	3179 ± 677	4785 ± 663	···	···	···
2008gi	···	···	···	···	···	···	···	···	···	···	···	···
2008gr	8832 ± 752	8361 ± 435	7548 ± 385	···	5412 ± 268	5013 ± 249	5918 ± 293	5572 ± 276	7487 ± 708	···	···	···
2008H	6608 ± 790	6734 ± 703	5355 ± 941	3863 ± 420	3791 ± 360	3738 ± 350	3821 ± 400	3678 ± 783	4669 ± 760	3390 ± 325	3430 ± 410	···
2008hg	···	···	···	···	···	···	···	···	···	···	···	···
2008ho	···	···	···	···	···	···	···	···	···	···	···	···
2008if	8534 ± 1126	8717 ± 549	7226 ± 642	3198 ± 200	4929 ± 298	4758 ± 398	5062 ± 272	4785 ± 251	7404 ± 633	3802 ± 189	4619 ± 234	4975 ± 515
2008il	···	···	···	···	···	···	···	···	···	···	···	···
2008in	4283 ± 721	4422 ± 768	3234 ± 310	2768 ± 259	2839 ± 373	2831 ± 455	2679 ± 283	2680 ± 251	2917 ± 321	2378 ± 203	2574 ± 227	2430 ± 266
2008K	7885 ± 619	7987 ± 793	6868 ± 701	···	6197 ± 352	5359 ± 437	···	5491 ± 301	7066 ± 501	···	···	···
2008M	6872 ± 862	6123 ± 631	5709 ± 474	3508 ± 214	3457 ± 345	3647 ± 458	3772 ± 271	3616 ± 198	4793 ± 1056	3388 ± 217	3507 ± 275	3040 ± 290
2008W	7013 ± 665	6016 ± 435	5873 ± 435	3455 ± 335	3743 ± 233	3846 ± 297	3733 ± 224	3506 ± 278	5244 ± 470	3094 ± 255	3314 ± 185	3100 ± 324
2009aj	3112 ± 455	2800 ± 183	2814 ± 470	2090 ± 161	2431 ± 197	2849 ± 315	···	···	3026 ± 240	···	···	200 ± 80

2009ao	5979 ± 859	6753 ± 544	5240 ± 471	3792 ± 334	3695 ± 256	3597 ± 210	4155 ± 206	3770 ± 230	4687 ± 335	...	3416 ± 170	3120 ± 290
2009au	2586 ± 524	2613 ± 215	1985 ± 165	1618 ± 113	1732 ± 161	1474 ± 175	1775 ± 237	1919 ± 296	1949 ± 118	1289 ± 64	1704 ± 85	1520 ± 130
2009bu	7400 ± 596	6430 ± 521	5567 ± 604	3996 ± 267	3975 ± 436	4034 ± 456	4233 ± 210	3460 ± 172	4378 ± 308	...	...	...
2009bz	...	...	...	...	...	...	...	...	...	...	...	...
2009N	4514 ± 377	4069 ± 909	2815 ± 259	2527 ± 282	2651 ± 299	2600 ± 439	2549 ± 238	2500 ± 195	2705 ± 186	2299 ± 206	2397 ± 156	2190 ± 185

Columns: (1) SN name; (2) Velocity of H_α absorption component; (3) Velocity of H_α emission component; (4) Velocity of H_β; (5) Velocity of Fe II λ4924; (6) Velocity of Fe II λ5018; (7) Velocity of Fe II λ5169; (8) Velocity of Fe II/Sc II; (9) Velocity of Sc II Multiplet; (10) Velocity of Na I D; (11) Velocity of Ba II; (12) Velocity of ScII; and (13) Velocity of O I.

Table 4 pEW values at 50 days from explosion

SN	H_α (Å)	H_α (Å)	H_β (Å)	Fe II λ4924 (Å)	Fe II λ5018 (Å)	Fe II λ5169 (Å)	Fe II/Sc II (Å)	Sc II Mult. (Å)	Na I D (Å)	Ba II (Å)	ScII (Å)	a/e
1986L	32.8 ± 4.1	144.2 ± 34.2	48.2 ± 3.6	1.2 ± 0.6	14.7 ± 1.8	36.7 ± 3.8	7.6 ± 2.9	10.4 ± 2.1	29.2 ± 2.7	0.0 ± 0.0	0.0 ± 0.0	0.23 ± 0.08
1988A	...	...	...	...	...	...	...	...	...	...	...	...
1990E	...	...	...	...	...	...	...	...	...	...	...	...
1990K	42.7 ± 3.8	206.2 ± 27.4	71.9 ± 4.4	0.0 ± 0.0	10.9 ± 0.7	38.8 ± 2.1	8.9 ± 0.7	13.2 ± 1.6	50.3 ± 2.5	6.4 ± 0.4	5.9 ± 0.9	0.21 ± 0.05
1991al	62.1 ± 5.8	214.2 ± 25.8	67.5 ± 5.2	4.8 ± 1.7	13.0 ± 1.7	27.2 ± 3.8	4.3 ± 1.9	6.5 ± 1.8	20.4 ± 1.2	6.4 ± 0.9	4.1 ± 1.2	0.29 ± 0.08
1992ad	...	...	...	...	...	...	...	...	...	...	...	...
1992af	...	...	...	...	...	...	...	...	...	...	...	...
1992am	...	...	...	...	...	...	...	...	...	...	...	...
1992ba	61.9 ± 4.2	119.3 ± 19.7	47.0 ± 3.9	7.6 ± 2.5	20.2 ± 2.5	30.1 ± 3.9	9.9 ± 1.5	13.7 ± 1.7	34.2 ± 3.7	7.9 ± 1.1	7.1 ± 0.9	0.52 ± 0.15
1993A	...	...	...	...	...	...	...	...	...	...	...	...
1993K	27.8 ± 3.8	126.1 ± 25.3	42.8 ± 2.7	6.4 ± 2.4	18.9 ± 3.8	28.7 ± 1.9	5.2 ± 1.2	7.3 ± 1.4	27.1 ± 1.9	3.8 ± 1	3.8 ± 1.1	0.22 ± 0.08
1993S	...	...	...	...	...	...	...	...	...	...	...	...
1999br	56.0 ± 3.1	14.6 ± 10.6	33.8 ± 4.8	15.0 ± 1.7	25.2 ± 1.5	43.1 ± 3.1	15.1 ± 2.9	20.8 ± 2	20.7 ± 1.9	12.9 ± 1.6	14.2 ± 1.0	3.84 ± 3.06
1999ca	48.3 ± 2.7	169.4 ± 13.6	78.9 ± 3.9	0.0 ± 0.0	17.6 ± 1.3	64.1 ± 2.9	11.1 ± 1.1	19.6 ± 1.7	33.7 ± 2.1	5.4 ± 0.4	11.6 ± 0.8	0.29 ± 0.03
1999cr	31.7 ± 4.2	137.5 ± 22.9	37.6 ± 4.1	0.0 ± 0.0	12.4 ± 1.7	24.9 ± 1.8	0.0 ± 0.0	6.4 ± 1.1	9.3 ± 2.2	0.0 ± 0.0	0.0 ± 0.0	0.23 ± 0.12
1999eg	...	...	...	...	...	...	...	...	...	...	...	...
1999em	75.8 ± 5.1	141.2 ± 40.2	40.3 ± 5.6	9.9 ± 1.6	23.8 ± 1.8	43.6 ± 2.5	11.7 ± 1.8	13.4 ± 2	30.6 ± 1.8	6.7 ± 1.0	7.5 ± 1.2	0.54 ± 0.25
S0210	36 ± 3.9	287.4 ± 42.3	83.5 ± 4.9	0.0 ± 0.0	30.4 ± 2.5	70.1 ± 3.5	7.8 ± 1.2	40.4 ± 3.3	49.2 ± 3.2	0.0 ± 0.0	0.0 ± 0.0	0.13 ± 0.06
2002ew	...	...	...	...	...	...	...	...	...	...	...	...
2002fa	45.4 ± 3.9	125.1 ± 43.6	52.4 ± 7.2	6.1 ± 1.1	15.5 ± 3.1	36.5 ± 2.4	9.7 ± 2.4	13.1 ± 2.4	42.4 ± 2.4	0.0 ± 0.0	0.0 ± 0.0	0.36 ± 0.21
2002gd	21.7 ± 3.3	106.8 ± 23.8	39.8 ± 3.3	5.8 ± 2.2	24.9 ± 3.5	59.3 ± 4.2	16.2 ± 2.8	26.9 ± 2.6	27.1 ± 5.1	3.8 ± 0.6	11.0 ± 2.1	0.20 ± 0.08
2002gw	61.4 ± 4.6	205.5 ± 29.5	58.4 ± 4.6	6.9 ± 1.6	18.2 ± 2.1	31.3 ± 2.7	5.5 ± 1.7	5.8 ± 2.0	13.5 ± 1.3	3.1 ± 1.1	3.8 ± 1.5	0.30 ± 0.11
2002hj	70.1 ± 5.3	207.5 ± 34.1	71.7 ± 5.5	2.8 ± 1.6	16.5 ± 2.9	40.8 ± 3.2	4.3 ± 2.5	10.2 ± 2.4	18.6 ± 1.9	0.0 ± 0.0	0.0 ± 0.0	0.34 ± 0.11
2002hx	88.8 ± 6.1	135.6 ± 18.1	73.8 ± 4.8	9.8 ± 2.2	20.8 ± 2.2	35.5 ± 3.0	7.5 ± 1.1	17.9 ± 1.7	53.1 ± 4.1	8.6 ± 1.2	1.3 ± 2.1	0.65 ± 0.16
2002ig	...	...	...	...	...	...	...	...	...	...	0.0 ± 0.0	...
2003B	60.1 ± 5.3	148.6 ± 27.6	53.0 ± 4.5	10.5 ± 1.8	23.4 ± 2.5	38.1 ± 2.3	14.2 ± 1.4	20.3 ± 2.4	28.6 ± 2.2	3.9 ± 0.9	8.8 ± 1.5	0.40 ± 0.11
2003bl	58.0 ± 4.3	116.5 ± 19.1	37.1 ± 2.1	15.1 ± 2.8	26.5 ± 2.5	38.3 ± 1.8	10.9 ± 2.9	17.0 ± 3.2	19.3 ± 1.6	11.7 ± 1.4	9.1 ± 1.9	0.51 ± 0.14
2003bn	77.7 ± 5.4	144.4 ± 66.6	55.3 ± 6.5	7.1 ± 1.9	17.3 ± 2.6	36.0 ± 1.1	8.3 ± 2.1	9.1 ± 1.4	16.1 ± 2.3	3.2 ± 1.0	2.5 ± 1.1	0.54 ± 0.36
2003ci	50.6 ± 2.5	166.2 ± 8.3	64.6 ± 3.2	1.3 ± 0.1	15.8 ± 0.8	46.2 ± 3.6	10.4 ± 0.5	20.7 ± 1.0	55.1 ± 1.8	7.7 ± 0.4	4.2 ± 0.2	0.31 ± 0.03
2003cn	43.7 ± 2.9	141.6 ± 18.4	52.9 ± 4.7	12.6 ± 2.1	21.1 ± 3.4	35.1 ± 2.9	9.2 ± 1.8	17.2 ± 1.3	18.2 ± 1.7	7.4 ± 1.5	7.1 ± 1.2	0.31 ± 0.06
2003cx	...	...	...	...	...	...	...	...	...	...	...	...
2003dq	...	...	...	...	...	...	...	...	...	...	...	...
2003E	...	...	...	...	...	...	...	...	...	...	...	...
2003ef	91.4 ± 7.3	130.5 ± 14.3	27.9 ± 4.2	9.8 ± 1.3	20.4 ± 1.7	28.3 ± 3.4	10.8 ± 2.9	9.4 ± 1.2	24.2 ± 1	1.9 ± 0.9	9.6 ± 1.2	0.70 ± 0.15
2003eg	9.4 ± 1.1	244.2 ± 24.5	60.6 ± 3.4	0.0 ± 0.0	14.4 ± 1.5	38.6 ± 1.1	10.5 ± 2.4	14.2 ± 1.7	58.4 ± 1.3	7.1 ± 1.1	6.5 ± 0.8	0.04 ± 0.01
2003ej	...	...	...	...	...	...	...	...	...	...	...	...
2003fb	73.7 ± 6.3	185.1 ± 13.4	55.1 ± 2.2	8.1 ± 0.8	18.1 ± 0.8	40 ± 2.3	7.9 ± 0.7	9.0 ± 1.1	25.0 ± 1.6	9.0 ± 1.8	7.1 ± 1.2	0.4 ± 0.06
2003gd	...	...	...	...	...	...	...	...	...	...	...	...
2003hd	78.1 ± 5.2	119.1 ± 30.9	56.8 ± 4.4	4.9 ± 1.1	16.1 ± 2.1	33.9 ± 2	4.6 ± 1.8	7.9 ± 0.7	15.4 ± 2.3	0.0 ± 0.0	0.0 ± 0.0	0.65 ± 0.26
2003hg	...	...	...	...	...	...	...	...	...	...	...	...
2003hk	32.6 ± 2.4	123.2 ± 12.4	39.2 ± 3.7	9.3 ± 2.9	17.6 ± 2.3	34.6 ± 2.6	0.0 ± 0.0	0.0 ± 0.0	44.3 ± 1.1	0.0 ± 0.0	0.0 ± 0.0	0.26 ± 0.18
2003hl	50.4 ± 3.1	118.3 ± 22.1	32.6 ± 5.9	6.8 ± 2.4	22.1 ± 2.9	39.5 ± 3.1	15.4 ± 1.9	19.2 ± 2.1	35.9 ± 2.5	5.6 ± 1.6	1.1 ± 1.2	0.43 ± 0.13
2003hn	61.4 ± 4.0	178.7 ± 22.4	60.0 ± 4.4	7.2 ± 1.1	17.5 ± 1.5	39.1 ± 3.7	10.2 ± 0.8	13.3 ± 1.5	31.5 ± 2.6	4.3 ± 0.9	5.3 ± 0.8	0.34 ± 0.07
2003ho	68.4 ± 4.8	269.8 ± 54.9	69.1 ± 4.6	5.4 ± 1.3	16.9 ± 1.9	42.7 ± 3.2	7.9 ± 1.1	8.3 ± 0.7	36.1 ± 1.9	0.0 ± 0.0	0.0 ± 0.0	0.25 ± 0.08
2003ib	...	...	...	...	...	...	...	...	...	...	...	...
2003ip	60.9 ± 4.2	191.4 ± 18.1	71.2 ± 6.8	0.0 ± 0.0	9.3 ± 2.2	43 ± 3.7	6.5 ± 1.4	12.0 ± 1.0	33.2 ± 2.6	4.9 ± 0.6	5.9 ± 1.1	0.32 ± 0.05
2003iq	84.2 ± 5.6	157.9 ± 14.4	46.2 ± 4.2	7.8 ± 2.1	21.3 ± 1.8	37.7 ± 3.1	10.4 ± 2.6	10.7 ± 0.9	32.3 ± 2.9	3.4 ± 1.2	6.0 ± 1.0	0.53 ± 0.13
2003T	58.5 ± 6	153.6 ± 29.6	27.6 ± 3.1	11.5 ± 3.7	22.9 ± 1.9	38.2 ± 3.6	14.0 ± 2.9	14.9 ± 1.3	35.1 ± 2.5	18.7 ± 6.7	10.2 ± 1.2	0.38 ± 0.21

2004dy	...	...	...	...	...	...	...	...	...	...	...	...
2004ej	57.1 ± 3.8	114.6 ± 20.3	48.6 ± 4.7	9.1 ± 2.1	20.7 ± 1.7	44.0 ± 4.3	14.7 ± 2.3	21.8 ± 2.9	37.2 ± 3.1	6.4 ± 1.6	5.9 ± 1.7	0.50 ± 0.17
2004er	74.4 ± 5.7	154.3 ± 23.7	59.2 ± 4.7	3.2 ± 1.5	10.7 ± 2.3	34.3 ± 2.8	3.6 ± 0.7	6.4 ± 1.4	16.2 ± 2.3	0.4 ± 0.6	2.6 ± 0.7	0.48 ± 0.14
2004fb	70.1 ± 7.2	165.5 ± 26.1	59.1 ± 3.4	6.9 ± 0.5	18.7 ± 2.1	46.9 ± 4.4	11.6 ± 1.2	16.8 ± 2.1	41.6 ± 2.8	10.8 ± 1.0	10.4 ± 1.2	0.42 ± 0.29
2004fc	34.8 ± 6.2	85.6 ± 37.9	16.2 ± 4.8	7.9 ± 2.1	18.7 ± 2.8	28.2 ± 3.1	10.2 ± 1.9	14.4 ± 1.7	23.1 ± 2.3	5.0 ± 1.1	6.6 ± 1.8	0.41 ± 0.36
2004fx	70.6 ± 4.7	168.9 ± 35.7	55.7 ± 3.3	8.6 ± 2.3	18.6 ± 3.1	30.7 ± 2.0	7.2 ± 2.5	4.4 ± 0.6	11.3 ± 1.2	2.7 ± 1.2	4.8 ± 1.4	0.42 ± 0.15
2005af	...	...	...	...	...	...	...	...	...	...	... ...	
2005an	51.9 ± 3.8	210.8 ± 27.1	74.4 ± 5.7	4.1 ± 0.4	15.4 ± 1.6	42.8 ± 2.9	12.1 ± 2.1	22.2 ± 2.5	18.4 ± 1.8	0.0 ± 0.0	10.5 ± 0.9	0.25 ± 0.06
2005dk	49.0 ± 3.3	166.6 ± 19.0	57.6 ± 3.5	5.4 ± 0.7	13.4 ± 1.2	32.7 ± 3.2	8.9 ± 2.3	11.1 ± 1.3	32.1 ± 1.6	4.2 ± 0.9	4.6 ± 0.9	0.29 ± 0.08
2005dn	66.6 ± 4.1	238.9 ± 54.3	77.9 ± 4.5	1.1 ± 2.2	3.9 ± 1.1	48.0 ± 3.1	0.0 ± 0.0	10.5 ± 1.2	30.7 ± 2.4	0.0 ± 0.0	0.0 ± 0.0	0.28 ± 0.09
2005dt	...	...	...	...	...	...	...	...	...	...	...	...
2005dw	...	...	...	...	...	...	...	...	...	...	...	...
2005dx	...	...	...	...	...	...	...	...	...	...	...	...
2005dz	77.2 ± 3.4	205 ± 41.1	50.4 ± 4.1	0.0 ± 0.0	20.3 ± 2.3	34.4 ± 2.8	0.0 ± 0.0	0.0 ± 0.0	0.0 ± 0.0	0.0 ± 0.0	0.0 ± 0.0	0.38 ± 0.141
2005es	...	...	...	...	...	...	...	...	...	...	...	...
2005J	77.2 ± 5.5	133.7 ± 30.3	64.0 ± 2.5	5.5 ± 1.8	15.9 ± 2.5	36.6 ± 2.4	8.6 ± 1.8	12.2 ± 1.4	23.2 ± 1.4	4.8 ± 1.7	3.9 ± 1.3	0.58 ± 0.201
2005K	...	...	...	...	...	...	...	...	...	...	...	...
2005lw	45.1 ± 4.2	210.0 ± 15.2	50.1 ± 3.4	0.0 ± 0.0	9.2 ± 1.5	60.0 ± 3.1	6.1 ± 1.7	7.0 ± 0.7	26.0 ± 2.1	3.5 ± 1.2	4.9 ± 1.6	0.21 ± 0.17
2005me	...	...	...	...	...	...	...	...	...	...	...	...
2005Z	65.9 ± 3.4	192.1 ± 35.7	56.8 ± 4.3	6.9 ± 1.5	12.7 ± 1.6	36.1 ± 3.7	10.4 ± 2.2	13.9 ± 1.6	49.2 ± 2.9	0.0 ± 0.0	0.0 ± 0.0	0.34 ± 0.118
2006ai	15.4 ± 2.6	173.2 ± 22.5	38.5 ± 3.4	3.2 ± 1.2	15.0 ± 2.1	36.8 ± 4.1	6.5 ± 2.5	7.8 ± 1.7	35.4 ± 2.1	0.0 ± 0.0	0.0 ± 0.0	0.09 ± 0.038
2006bc	...	...	...	...	...	...	...	...	...	...	...	...
2006be	62.2 ± 3.3	180.5 ± 7	68.1 ± 3.0	5.6 ± 1.3	15.1 ± 0.7	26.0 ± 2.1	8.0 ± 1.2	12.0 ± 1.2	20.0 ± 1.2	5.3 ± 1.0	0.0 ± 0.0	0.34 ± 0.037
2006bl	...	...	...	...	...	...	...	...	...	...	...	...
2006ee	62.6 ± 6.2	122.1 ± 22.5	24.5 ± 4.5	15.2 ± 3.2	26.6 ± 2.9	42.4 ± 2.8	14.6 ± 1.5	18.1 ± 2.2	39.1 ± 2.8	13.1 ± 1.8	14.1 ± 1.2	0.51 ± 0.227
2006it	...	...	...	...	...	...	...	...	...	...	...	...
2006iw	40.6 ± 4.2	94.7 ± 12.2	38.1 ± 3.3	3.5 ± 1.6	10.0 ± 0.7	16.0 ± 1.6	5.0 ± 0.8	6.7 ± 1.2	12.1 ± 2	0.0 ± 0.0	0.0 ± 0.0	0.43 ± 0.097
2006ms	...	...	...	...	...	...	...	...	...	...	...	...
2006qr	69.7 ± 4.6	133.1 ± 15.1	61.9 ± 5.3	11.5 ± 0.6	22.1 ± 1.9	44.0 ± 4.2	16.3 ± 3.1	20.2 ± 2.6	33.6 ± 2.4	8.8 ± 1.9	12.6 ± 1.2	0.52 ± 0.214
2006Y	10.4 ± 2.9	123.7 ± 27.3	25.5 ± 2.8	1.6 ± 0.5	6.7 ± 1.8	16.3 ± 3.1	0.0 ± 0.0	0.0 ± 0.0	15.8 ± 1	0.0 ± 0.0	0.0 ± 0.0	0.08 ± 0.042
2007aa	74.5 ± 6.5	119.7 ± 11.0	52.5 ± 5.8	9.6 ± 1.1	20.7 ± 1.8	35.1 ± 2.5	10.7 ± 2.1	13.1 ± 1.5	31.8 ± 2.9	1.1 ± 0.9	5.7 ± 1.6	0.62 ± 0.145
2007ab	72.4 ± 5.1	232.1 ± 26.4	84.6 ± 5.4	0.0 ± 0.0	17.5 ± 3.6	77.2 ± 3.4	6.6 ± 2.6	23.0 ± 2.4	32.9 ± 2	8.0 ± 1.1	12.0 ± 2.3	0.31 ± 0.083
2007av	97 ± 6.6	164.9 ± 22.2	46.4 ± 3.3	8.6 ± 1.5	21.8 ± 1.4	43.9 ± 2.5	10.9 ± 2.8	12.3 ± 1.8	29.4 ± 3.2	7.6 ± 1.9	8.3 ± 1.5	0.59 ± 0.119
2007bf	...	...	...	...	...	...	...	...	...	...	...	...
2007hm	44.1 ± 4.3	180.7 ± 36.8	56.2 ± 5.9	8.3 ± 0.7	16.6 ± 3.3	29.1 ± 3.3	9.8 ± 1.6	14.3 ± 1.4	22.3 ± 2.2	0.0 ± 0.0	0.0 ± 0.0	0.24 ± 0.105
2007il	63.9 ± 5.4	190.2 ± 36.5	66.4 ± 4.2	2.8 ± 2.1	13.4 ± 2.5	28.2 ± 6.3	0.0 ± 0.0	0.0 ± 0.0	15.6 ± 1.1	0.0 ± 0.0	0.0 ± 0.0	0.34 ± 0.114
2007it	...	...	...	...	...	...	...	...	...	...	...	...
2007ld	...	...	...	...	...	...	...	...	...	...	...	...
2007oc	35.5 ± 2.8	267.1 ± 22.4	70.1 ± 6.9	4.5 ± 1.5	8.0 ± 1.9	46.5 ± 4.6	4.3 ± 1.9	14.4 ± 1.9	43.6 ± 1.8	3.5 ± 1.5	2.9 ± 1.0	0.13 ± 0.022
2007od	32.9 ± 3.1	184.0 ± 22.5	65.2 ± 5.1	0.0 ± 0.0	14.7 ± 2.7	36.0 ± 3.8	0.0 ± 0.0	15.2 ± 1.7	16.4 ± 0.9	3.5 ± 0.6	5.3 ± 1.4	0.18 ± 0.039
2007P	...	...	...	...	...	...	...	...	...	...	...	...
2007sq	37.5 ± 4.2	125.9 ± 36.4	48.3 ± 4	4.52 ± 1	6.8 ± 1.9	31.8 ± 3.5	5.1 ± 1.7	7.7 ± 0.9	22.4 ± 0.9	0.0 ± 0.0	0.0 ± 0.0	0.30 ± 0.167
2007U	31.1 ± 3.2	142.8 ± 32.4	54.3 ± 4.2	0.0 ± 0.0	12.0 ± 2.1	40.9 ± 2.3	10.0 ± 2.1	15.6 ± 2.1	17.1 ± 1.7	0.0 ± 0.0	0.0 ± 0.0	0.22 ± 0.079
2007W	67.2 ± 3.6	131.2 ± 21.7	38.1 ± 5.9	11.52 ± 2	21.7 ± 2.6	36.5 ± 2.8	10.2 ± 2.6	16.0 ± 1.8	13.5 ± 2.2	4.6 ± 1.3	4.1 ± 1.3	0.51 ± 0.127
2007X	45.2 ± 2.8	223.8 ± 32.8	77.1 ± 4.7	0.0 ± 0.0	13.9 ± 2.9	49.4 ± 2.1	10.3 ± 3.2	16.4 ± 1.6	22.9 ± 1.2	5.6 ± 0.9	9.1 ± 1.4	0.20 ± 0.06
2007Z	...	...	...	...	...	...	...	...	...	...	...	...
2008ag	60.6 ± 5.2	185.2 ± 15.8	39.3 ± 3.2	10.7 ± 2.1	22.3 ± 1.7	38.9 ± 2.6	10.1 ± 1.9	14.6 ± 1.7	38.4 ± 2.1	3.3 ± 1.8	5.5 ± 1.2	0.33 ± 0.072
2008aw	17.8 ± 2.3	175.8 ± 18.8	47.1 ± 4.6	3.1 ± 1.3	12.4 ± 1.4	37.8 ± 1.4	6.4 ± 1.2	8.2 ± 0.6	38.8 ± 2.9	3.6 ± 1.6	3.6 ± 1.3	0.10 ± 0.051
2008bh	55.8 ± 4.2	216.8 ± 41.7	54.4 ± 5.6	4.7 ± 1.3	16.2 ± 2.0	36.2 ± 1.1	8.3 ± 2.2	9.8 ± 1.0	16.7 ± 1.9	5.2 ± 0.9	5.2 ± 0.8	0.26 ± 0.101
2008bk	57.5 ± 4.8	94.3 ± 12.0	31.9 ± 3.9	16.3 ± 1.2	24.6 ± 2.1	43.7 ± 3.5	14.8 ± 1.7	21.8 ± 2.1	20.1 ± 1.7	11.8 ± 1.2	10.5 ± 1.1	0.61 ± 0.16
2008bm	4.6 ± 0.2	16.1 ± 0.8	19.2 ± 1.3	9.1 ± 0.5	11.6 ± 0.6	19.8 ± 2.1	0.0 ± 0.0	0.0 ± 0.0	3.4 ± 0.6	0.0 ± 0.0	0.0 ± 0.0	0.29 ± 0.027
2008bp	...	...	...	...	...	...	...	...	...	...	...	...
2008br	15.8 ± 3.0	23.3 ± 17.9	22.3 ± 3.2	7.1 ± 1.8	7.2 ± 1.1	9.7 ± 2.8	8.8 ± 1.9	12.9 ± 1.1	12.4 ± 0.7	9.4 ± 1.1	6.7 ± 2.5	0.69 ± 0.752

2008bu	...	...	...	...	...	...	...	...	...	...	...	...
2008F	...	...	...	...	...	...	...	...	...	...	...	...
2008ga	85 ± 5.7	234.1 ± 13.2	60.0 ± 2.3	6.8 ± 1.5	17.0 ± 1.5	35.1 ± 2.1	7.1 ± 1.8	15.0 ± 1.7	55.0 ± 2.1	0.0 ± 0.0	0.0 ± 0.0	0.36 ± 0.045
2008gi	...	...	...	...	...	...	...	...	...	...	...	...
2008gr	35.5 ± 3.5	186.4 ± 41.5	56.6 ± 3.6	0.0 ± 0.0	7.3 ± 0.9	34.1 ± 2.6	4.7 ± 1.8	7.8 ± 1.0	30.9 ± 2.5	0.0 ± 0.0	0.0 ± 0.0	0.19 ± 0.099
2008H	63.3 ± 5.1	150.2 ± 21.0	33.0 ± 3.1	10.0 ± 2.1	22.2 ± 1.7	51.0 ± 3.2	14 ± 1.9	20.0 ± 2.1	54.1 ± 3.1	15.0 ± 2.2	14.0 ± 1.8	0.42 ± 0.132
2008hg	...	...	...	...	...	...	...	...	...	...	...	...
2008ho	...	...	...	...	...	...	...	...	...	...	...	...
2008if	26.1 ± 2.3	239.2 ± 58.9	61.8 ± 3.7	2.4 ± 1.1	9.3 ± 1.3	30.2 ± 3.3	4.7 ± 1.2	6.9 ± 1.3	48.3 ± 3.2	1.2 ± 0.5	3.7 ± 0.9	0.11 ± 0.06
2008il	...	...	...	...	...	...	...	...	...	...	...	...
2008in	54.8 ± 7.3	157.6 ± 49.6	36.6 ± 3.1	14.5 ± 3.1	26.9 ± 1.9	42.9 ± 2.7	14.7 ± 2.6	18.3 ± 1.4	38.8 ± 2.3	6.4 ± 1.4	8.3 ± 1.8	0.35 ± 0.22
2008K	40.5 ± 4.5	250.8 ± 44.5	80.4 ± 4.2	0.0 ± 0.0	17.4 ± 2.6	62.8 ± 1.8	0.0 ± 0.0	19.1 ± 2.1	41.5 ± 3.1	0.0 ± 0.0	0.0 ± 0.0	0.16 ± 0.07
2008M	54.0 ± 5.5	208.7 ± 27.7	72.9 ± 3.8	5.3 ± 2.1	20.2 ± 3.4	34.0 ± 1.9	4.9 ± 2.1	7.5 ± 1.4	30.3 ± 2.8	2.5 ± 0.9	1.6 ± 1.1	0.26 ± 0.06
2008W	46.7 ± 4.2	200.2 ± 21.9	60.4 ± 3.4	5.1 ± 1.9	16.4 ± 2.9	36.9 ± 2.8	7.7 ± 1.9	12.7 ± 1.1	45.9 ± 1.7	3.5 ± 1.4	4.6 ± 1.7	0.23 ± 0.08
2009aj	8.1 ± 1.6	46.7 ± 6.1	13 ± 2.2	6.2 ± 1.6	8.5 ± 0.9	13.9 ± 3.1	0.0 ± 0.0	0.0 ± 0.0	1.7 ± 0.6	0.0 ± 0.0	0.0 ± 0.0	0.17 ± 0.06
2009ao	40.2 ± 3.1	148.6 ± 11	54.5 ± 3.4	5.8 ± 6.2	18.5 ± 1.4	41.8 ± 2.7	9.3 ± 1.6	19.4 ± 2.1	24.2 ± 1.6	0.0 ± 0.0	9.1 ± 1.8	0.27 ± 0.04
2009au	5.9 ± 1.4	34.3 ± 11.1	12.8 ± 2.7	8.8 ± 2.8	11.9 ± 1.7	17.2 ± 2.5	6.1 ± 1.8	7.3 ± 2.3	7.9 ± 0.8	3.3 ± 0.6	5.6 ± 1.3	0.17 ± 0.09
2009bu	84.6 ± 5.3	146.5 ± 23.3	55.9 ± 3.1	3.6 ± 1.1	14.2 ± 1.9	26.4 ± 1.8	5.7 ± 2.2	6.1 ± 2.5	15.1 ± 1.5	0.0 ± 0.0	0.0 ± 0.0	0.58 ± 0.14
2009bz	...	...	...	...	...	...	...	...	...	...	...	...
2009N	75.7 ± 3.1	118.5 ± 20.7	39.1 ± 3.9	15.2 ± 1.9	25.4 ± 1.6	34.4 ± 2.1	13.7 ± 1.1	20.8 ± 2.1	24.5 ± 1.2	10.3 ± 1.6	9.6 ± 1.1	0.64 ± 0.22
2009W	...	...	...	...	...	...	...	...	...	...	...	...

Columns: (1) SN name; (2) pEW of H_α absorption component; (3) pEW of H_α emission component; (4) pEW of H_β; (5) pEW of Fe II λ4924; (6) pEW of Fe II λ5018; (7) pEW of Fe II λ5169; (8) pEW of Fe II/Sc II; (9) pEW of Sc II Multiplet; (10) pEW of Na I D; (11) pEW of Ba II; (12) pEW of ScII; (13) Ratio of absoprtion to emission (a/e) of H_α P-Cygni profile.